Tectonophysics 862 (2023) 229980

Contents lists available at ScienceDirect

Tectonophysics

journal homepage: www.elsevier.com/locate/tecto

Iapetus Ocean serpentinites and Mesozoic intra-platform basins revealed by gravity and magnetic modelling across the Greater East Shetland Platform (Northern North Sea, UK)

Mattia De Luca [a,*], Paolo Mancinelli [a], Stefano Patruno [b], Vittorio Scisciani [a]

[a] Department of Engineering and Geology, G. d'Annunzio University of Chieti and Pescara, Via dei Vestini 31, Chieti, Italy
[b] Department of Engineering, School of Sciences and Engineering, University of Nicosia, Nicosia, Cyprus

ARTICLE INFO

Keywords:
Gravity and magnetic forward modelling
Mesozoic Basins
Caledonian Orogeny
Greater East Shetland Platform

ABSTRACT

The Greater East Shetland Platform and its intra-platform basins (i.e. the Dutch Bank Basin and East Orkney Basin) are examples of poorly explored areas in the UK Continental Shelf (Northern North Sea), hosting a locally thick (1–8 km) Devonian-to-Tertiary sedimentary succession that unconformably overlies the Caledonian crystalline basement.

Starting from a grid of seismic reflection lines, six recently acquired profiles were selected, interpreted and depth-converted. The resulting geological cross sections were integrated with forward modelling of the observed Bouguer gravity and magnetic anomalies, and constrained by the available wellbore-derived petrophysical parameters.

Our seismic interpretation and modelling suggest that the first-order contributors to the observed Bouguer gravity anomalies are related to the scattered distribution of the Mesozoic sedimentary sequences in the intra-platform basins. Furthermore, the main sources of the modelled magnetic anomalies are related to high-susceptibility (≤0.05 SI units) bodies in the crustal basement that locally correspond to zones of high reflectivity imaged in the seismic profiles. Such deep sources are interpreted as paleo-domains inherited from the pre-Devonian tectonic evolution of the study area and assembled during the Caledonian Orogeny. This may be relatable to the offshore extension of first-order pre-Devonian tectonic lineaments exposed in the Scottish Highlands and Orkney-Shetland islands.

1. Introduction

The combined modelling of gravity and magnetic anomalies can significantly contribute to the understanding of subsurface geology, particularly if constrained by the field geology and/or by well-data and seismic profiling (e.g., Garland, 1951; Telford et al., 1990; Düzgit et al., 2006; Rybakov et al., 2011; Mancinelli et al., 2020; Mancinelli et al., 2022). Moreover, this method of study becomes crucial to define the subsurface framework when some of such external constraints are lacking or sparse as in the Greater East Shetland Platform (GESP – sensu Patruno and Reid, 2016) in the Northern North Sea (NNS), which is the focus area of this work (Fig. 1).

Hydrocarbon-oriented exploration of this area has been historically less developed than in other surrounding basins (e.g., the Viking Graben) due to the early interpretations of this continental platform as a tectonic high with shallow acoustic basement and rare mature source rocks (Platt, 1995; Platt and Cartwright, 1998; Zanella and Coward, 2003). As a consequence, the GESP area was investigated by only few regional studies. These were based on deep seismic profiles (White, 1989; McBride and England, 1999), sometimes combined with gravity and magnetic modelling (Holliger and Klemperer, 1989; Holliger and Klemperer, 1990; Fichler and Hospers, 1990; Fichler et al., 2011; Arsenikos et al., 2016; Kimbell and Williamson, 2016; Frogtech Geoscience, 2017; Patruno et al., 2017; Karstens et al., 2022).

The study area is approximately 33×10^3 km^2 and includes the UK quadrants 1–2, 5–9, 12–15 (Fig. 1). It is located in the UK NNS and corresponds to a large-scale Mesozoic platform to the east of the alignment of the Caithness headland – Orkney Island – Fair Isle – Shetland Island – Unst Basin, to the west of the Viking Graben and East Shetland Basin, and to the north of the Moray Firth Basin and Witch Ground

* Corresponding author.
E-mail address: mattia.deluca@unich.it (M. De Luca).

https://doi.org/10.1016/j.tecto.2023.229980
Received 21 February 2023; Received in revised form 3 June 2023; Accepted 22 June 2023
Available online 3 July 2023

Graben (Fig. 1b). This area is interposed between the outcropping British and Scandinavian Caledonian orogen and is thought to include the north-eastward continuation of the Highland terranes and intervening boundary faults closely exposed in Scottish mainland (Strachan and Woodcock, 2021). Due to the overprint of the Mesozoic rifting onto the pre-existing Caledonian sutures, the limits between Laurentia, Baltica and Avalonia plates involved in the Caledonian collision are poorly constrained and they remain masked underneath a thick pile of the North Sea rift and post-rift sediments (Soper et al., 1992; Turner et al., 2018; Patruno et al., 2022). Despite the relevant reconstructions close to land exposures by deep seismic-reflection profiles around the UK, Ireland, and eastern North Sea (NW of Denmark – Beamish and

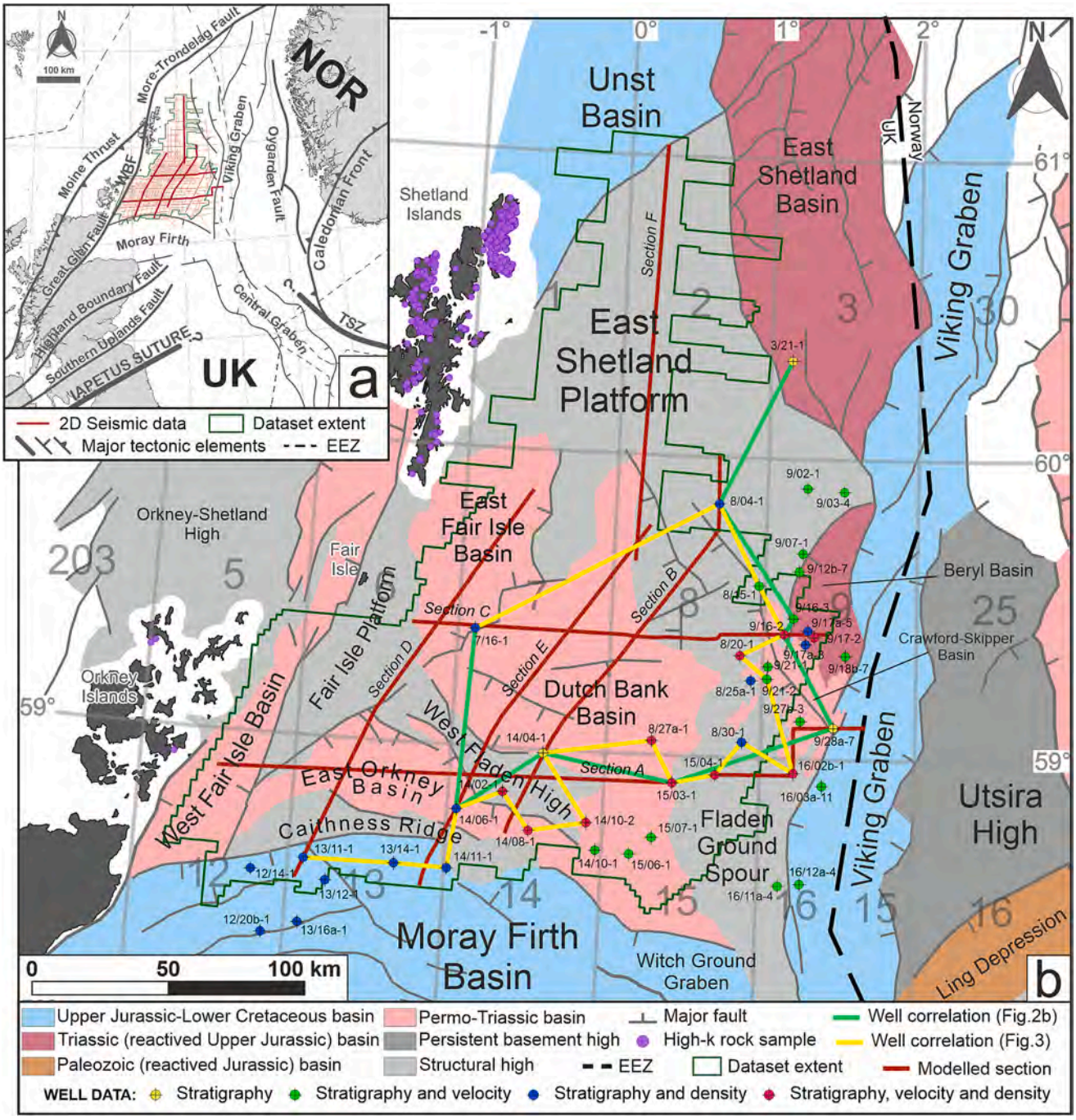

Fig. 1. (a) Location of the grid of 2D seismic profiles (thin red lines) from the PP162DGOGA survey (NSTA, 2022) and high resolution gravity-magnetic dataset (delimited by green line) in the UK sector of the NNS. Simplified tectonic lineaments modified from Zanella and Coward (2003) and Strachan and Woodcock (2021). WBF, Walls Boundary Fault; TSZ, Tornquist Fault Zone. (b) Regional structural scheme showing the main Paleozoic-Mesozoic basins and structural highs in the NNS modified from Scisciani et al., 2021). Dataset extent indicates the extension of the Bouguer gravity and magnetic anomaly data from Bliss et al. (2016). Traces of seismic lines and geological cross-sections modelled in this work are in red; seismic profiles were retrieved from the National Data Repository (NDR) of NSTA (2022). Violet dots show the distribution of onshore gabbroic, serpentinite and serpentinized rock samples (BGS, 2022) that can be related to high magnetic susceptibility (high-k rock samples). EEZ, exclusive economic zone; UK, United Kingdom; NOR, Norway. Original name of the sections: Section A – 228A045_EXTRA_C, Section B – 045B028 EXTRA-A, Section C – 024A024 EXTRA-B, Section D – OA16ESP00039A032, Section E – OA16ESP00109A011, Section F – OA16ESP00091A093. (For interpretation of the references to colour in this figure legend, the reader is referred to the web version of this article.)

Smythe, 1986; Soper et al., 1992; Abramovitz and Thybo, 2000), the prolongation of the British-Irish Caledonian Terranes and the intervening main faults (e.g., the Great Glen Fault, Highland Boundary Fault and Southern Upland Fault – Fig. 2a – Flinn, 1961; Flinn, 1992; Strachan and Woodcock, 2021) in the GESP and their relationship with the Scandinavian Caledonides remains unclear and it is still matter of debate (Coward et al., 2003).

In this work, we provide a first-order geological and geophysical investigation of the main sedimentary basins in the GESP and the interpretation of nature and geometries of deeper bodies within the crust. In particular for the shallower basins, we focus on the still underexplored Dutch Bank Basin, the East Orkney Basin and East Fair Isle Basin (Fig. 1b), together with their related fault-bounded structural highs – i.e. the Caithness Ridge, Fair Isle Platform and the West Fladen High (Fig. 1b – Johnson et al., 2005; Richardson et al., 2005; Patruno and Reid, 2016; Patruno and Reid, 2017; Arsenikos et al., 2016; Arsenikos et al., 2018; Kimbell and Williamson, 2016; Patruno et al., 2019; Scisciani et al., 2021).

2. Tectonic and geological setting

2.1. Tectonic setting

Starting from Cambrian times, the study region experienced alternating phases of compressional and extensional tectonics, separated by periods of relative tectonic quiescence (e.g., Patruno and Scisciani, 2021). The main compressional phase occurred during the Caledonian Orogeny (Silurian-Early Devonian) which was preceded by the closure of the previously rifted apart margins of the East Iapetus Ocean (Robert et al., 2021) and the collision of Laurentia with Avalonia and Baltica plates (Soper et al., 1992; Turner et al., 2018; Patruno et al., 2022). The assemblage and exhumation of the Caledonian orogen was accompanied by multiple plutonic intrusions (Atherton and Ghani, 2002, and references therein) and by later Devonian extensional collapse or strike-slip reworking (McClay et al., 1986; Coward et al., 1989; Seranne et al., 1989). The Devonian tectonics led to the development of widespread and deep basins infilled by thick wedges of "Old Red Sandstone" (Steel et al., 1985) in western Scandinavia, Northern Scotland and neighbouring offshore areas (e.g., East Shetland Platform and West Shetland Basin; Norton, 1987; Osmundsen et al., 1998; Seranne and Seguret, 1987; Fossen, 1992; Platt and Cartwright, 1998; Marshall and Hewett, 2003; Fossen and Hurich, 2005; Fossen, 2010; Wilson et al., 2010; Vetti and Fossen, 2012; Bird et al., 2015; Fossen et al., 2016; Phillips et al., 2016; Patruno et al., 2019; Scisciani et al., 2019; Scisciani et al., 2021; Patruno et al., 2022). The Devonian basins were later affected by a regional inversion tectonic phase in the Upper Carboniferous (Platt, 1995; Platt and Cartwright, 1998; Patruno et al., 2019), concurrently with the Variscan Orogeny (Ziegler, 1975).

Since early Permian times, the area underwent multiple extensional events which culminated in the Late Jurassic-Cretaceous North Sea rifting (Zanella and Coward, 2003; Johnson et al., 2005). During the Middle Jurassic, a further magmatic and erosional event (Aalenian Mid North Sea doming – Underhill and Partington, 1993) affected the Caledonian terranes and preceded the subsequent rift development (Ziegler, 1992; Fraser et al., 2003; Patruno et al., 2022).

During Tertiary, the post Mesozoic-rifting subsidence was interrupted by localised Alpine-age compressional events and contemporaneously large-scale epeirogenic uplift affected the rift margins with erosion of vast area in the UK (White, 1989; Glennie and Underhill, 1998; Smallwood et al., 1999; Smallwood and White, 2002).

2.2. Geological and structural setting of the GESP and adjacent onshore areas

NW and SW of the GESP, there are outcropping metamorphic and plutonic rocks which form the ground of the mainland Scottish Caledonides (Lambert and McKerrow, 1976; Dewey and Shackleton, 1984; Strachan et al., 2002). In particular, the study area extends east of the Walls Boundary Fault (Fig. 1a), a main lineament trending approximately NNE-SSW from the west Orkney Islands through the Shetland Islands (Seranne, 1992; Flinn, 1992). This fault was previously thought to have accommodated significant left-lateral movement and it is interpreted as the north-eastern extension of the Great Glen Fault (Fig. 1a), along which an analogous horizontal movement has been documented (Andrews et al., 1990; Underhill and Brodie, 1993; Stewart et al., 1999; Roberts and Holdsworth, 1999; Dewey and Strachan, 2003; Mendum and Noble, 2010). The Great Glen Fault separates the Moine from the Dalradian terranes and it accommodated horizontal deformation during the Caledonian orogeny before being reactivated in more recent times (Hutton and McErlean, 1991; Stewart et al., 1997; Le Breton et al., 2013; Armitage et al., 2021). The Dalradian Group was deposited on the south-eastern margin of Laurentia and was affected by at least two rifting episodes that culminated with the opening of the Iapetus Ocean ca. 600 Ma (Soper and England, 1995; Dewey et al., 2015). Similar *syn*-rift successions, referred to the Dalradian block, are also exposed in the north-eastern Shetland Islands, where they are tectonically overlaid along a Caledonian thrust fault to the Shetland Ophiolite Complex (e.g., Prichard and Lord, 1993; Flinn, 2001). This complex consists of two thrust-bounded nappes composed of mafic and ultramafic igneous rocks, with associated low-grade metasedimentary rocks and mélanges that include both basic and metavolcanic rocks (Flinn, 1999; Flinn et al., 2013 and references therein). The Shetland ophiolites are thought to be obducted onto the Laurentian continental margin during Ordovician times (Grampian Orogeny – Crowley and Strachan, 2015) and then telescoped onto the Dalradian terrane during the Silurian-age Scandian orogenic event following the westward movement and collision of Baltica (Flinn and Oglethorpe, 2005). The Shetland Ophiolite Complex is now recognised as a fragment of the Iapetus Ocean or most likely a related marginal basin and it shows several analogies in composition, structural setting and age with a chain of ophiolite fragments found throughout the Laurentian Caledonides of the British Isles and occurring along the Highland Border in Scotland and on the west coast of Ireland (Williams and Smyth, 1973; Flinn, 1999, and references therein). Several lines of evidence suggest that ophiolites were formed in supra-subduction zone arc–forearc settings shortly prior to orogenesis and then thrust (obducted) onto a colliding passive margin. These ophiolites were emplaced during the early to mid-Ordovician Grampian orogenic event, which records the initial stages in closure of the Iapetus Ocean (Chew et al., 2010). The collision of a juvenile oceanic arc with the Laurentian passive margin resulted in NW-directed ophiolite obduction (present reference frame) with regional deformation and metamorphism of footwall metasedimentary successions (e.g., Dewey and Shackleton, 1984; Chew et al., 2010).

In the GESP, the basement was rarely penetrated by exploration wells and the few available logs report high grade metamorphic rocks and numerous intrusive bodies, including Devonian granites penetrated at the eastern edge of the GESP (e.g., Well 3/21–1 on Fig. 1 – Donato and Tully, 1982; Holloway et al., 1991; Bassett, 2003; Patruno and Reid, 2016; Whitbread and Kearsey, 2016; Patruno and Reid, 2017; Arsenikos et al., 2018; Patruno et al., 2019; Kombrink and Patruno, 2020). Southeast of the GESP, Middle Jurassic mafic effusive and volcaniclastic sequences were encountered by wells and imaged by seismic reflection in the Rattray Volcanic Province at the triple junction of the Mesozoic North Sea rift system (e.g., Quirie et al., 2018). High-susceptibilities rocks were reported in the ophiolites of the Shetland islands (e.g., gabbroid and serpentinized rocks – Flinn, 1996 and references therein). These mafic rocks are interpreted, with intermediate intrusives, in the lower crust north-east of the British Isles, where they are presumably related to an island-arc system pertaining to the Iapetus Ocean (Fichler et al., 2011). Similar mafic rocks, seemingly buried under granitoid rocks, were reported at the bottom of a few hydrocarbon wells in the offshore East Shetland Platform (e.g., hornblend-biotite schists with

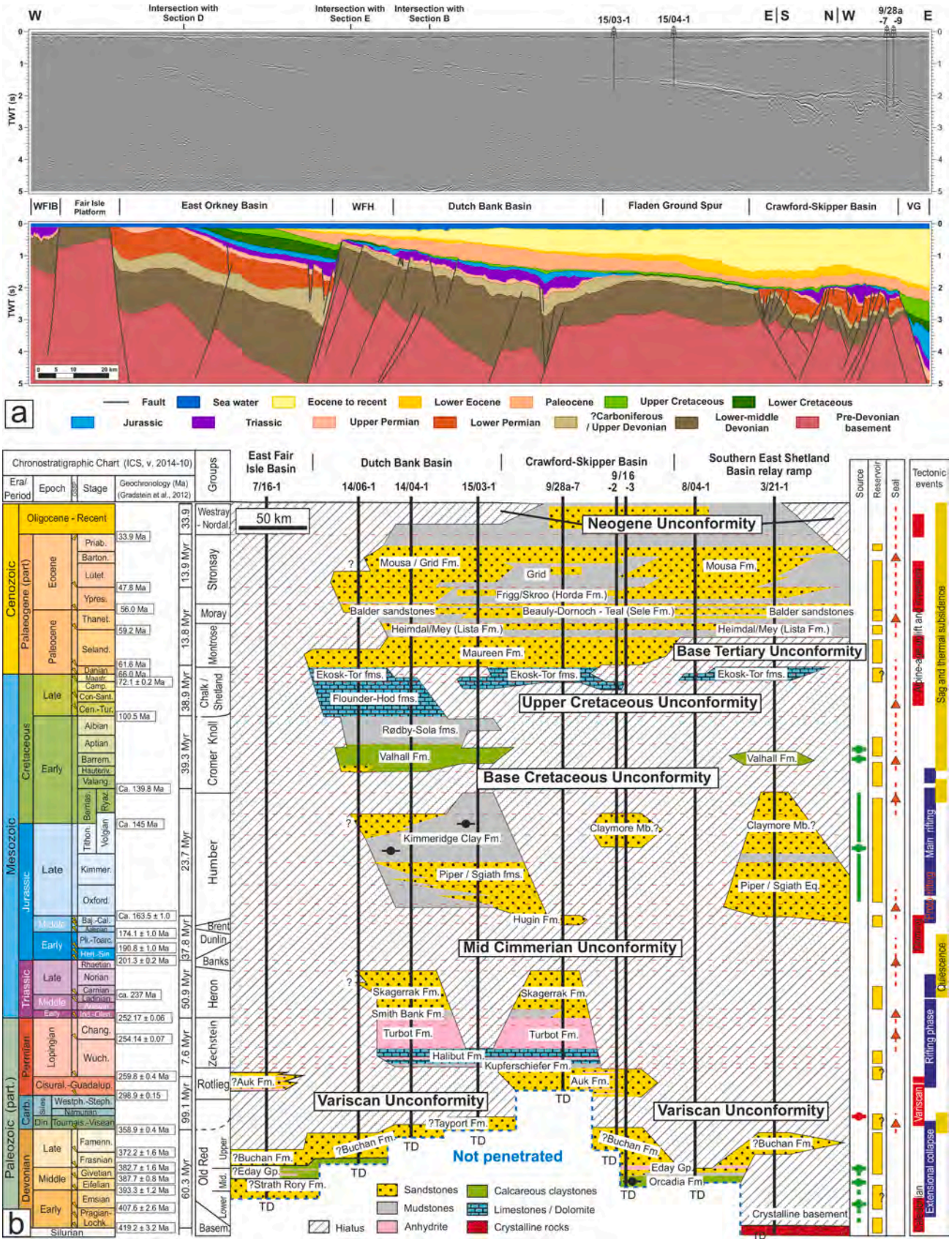

Fig. 2. (a) Uninterpreted and interpreted version of the regional seismic reflection profile (Section A in Fig. 1b for location) showing the different ages and thickness distribution of sedimentary basins overlaying the metamorphic basement. (b) Regional chronostratigraphic and lithostratigraphic correlation panel of wells (green line in Fig. 1b) showing the inhomogeneous lateral and vertical distribution of the sedimentary cover and unconformities related to the main tectono-magmatic events (modified from Scisciani et al., 2021). WFIB, West Fair Isle Basin; WFH, West Fladen High; VG, Viking Graben. (For interpretation of the references to colour in this figure legend, the reader is referred to the web version of this article.)

metamorphic cooling age of 393 Ma described in Well 9/04a-1 by Bassett, 2003; Patruno et al., 2017; Scisciani et al., 2019).

Recent revision of the available well-log and interpretation of seismic reflection data in the GESP (Patruno and Reid, 2016; Patruno and Reid, 2017; PGS, 2017; Patruno et al., 2019; Scisciani et al., 2019; Scisciani et al., 2021) revealed a laterally discontinuous but locally thick (up to 7–8 km) sedimentary cover, unconformably overlaying the Caledonian igneous and metamorphic basement (Fig. 2). This sedimentary sequence mainly consists of easterly tilted Devonian-to-Cretaceous deposits overlain by a wedge-shaped and west-northwesterly thinning Cenozoic units (Fig. 2a).

Underneath the Tertiary unit, the GESP is arranged in several structural highs (Fig. 1b) with different attitudes (including the *E*-W trending Caithness Ridge, the SSW-NNE trending Fair Isle Platform, the NW-SE trending West Fladen High, NW-SE trending East Shetland Platform and the N-S trending Fladen Ground Spur) separated by intervening late Paleozoic and Mesozoic basins (Fig. 2a – East Orkney Basin, Dutch Bank Basin, West Fair Isle Basin, East Fair Isle Basin, Crawford-Skipper Basin – Andrews et al., 1990; Platt, 1995; Platt and Cartwright, 1998; Richardson et al., 2005; Patruno and Reid, 2016; Patruno and Reid, 2017; Scisciani et al., 2021).

Field exposures in north-western Britain (e.g., Orcadian Basin) and wells penetration in the GESP or in the Moray Firth Basin indicate Devonian sediments of the Old Red Sandstone Group at the base of the sedimentary cover unconformably overlaying the Caledonian basement (Marshall and Hewett, 2003; Kendall, 2017; Whitbread and Kearsey, 2016; Marshall et al., 2019).

This interval consists of Devonian sediments (Fig. 2) with sandstone-rich continental deposits (e.g., upper Devonian Buchan Formation – Fm.), marls, lacustrine mudstones, marine anhydrite-dolomite markers (e.g., middle Devonian Eday Group – Gp., Strath Rory Fm. and Orcadia Fm.), and Lower Devonian fluvial sandstones with thick conglomerates (Marshall and Hewett, 2003; Patruno et al., 2019).

In the GESP, Carboniferous units have only been preserved in the Dutch Bank Basin and Piper Shelf depocenters (e.g., wells 14/08–1, 8/27a-1), a fact which suggest uplift and erosion of large sector of the platform during this times (Patruno and Reid, 2016; Patruno and Reid, 2017). In fact, the succession composed of lower-upper Permian Rotliegend Group and a thin uppermost Permian Zechstein is directly underlain by the Base Permian Unconformity, which reflects the Upper Carboniferous Variscan uplift and inversion tectonics (Fig. 2b – Patruno et al., 2019; Scisciani et al., 2021). These units are respectively represented by the sandstones of the Auk Fm. at the base (e.g., well 9/28a-7 in the Crawford-skipper Basin) and the carbonate-evaporite cyclothems of the Zechstein Group at the top (well 9/28a-7 – Glennie et al., 2003; Patruno and Reid, 2017; Patruno et al., 2019).

Throughout the GESP, Triassic deposits are confined into *syn*-tectonic intra-platform extensional fault-related basins (Figs. 1 and 2 – Johnson et al., 2005; Patruno and Reid, 2017; Scisciani et al., 2021) and tend to conformably overlie the Zechstein Gp. (e.g., Patruno et al., 2019). The lower facies comprise lacustrine and alluvial claystone of the Smith Bank Fm., overlain by the fluvial sandstones of the Skagerrak Fm. (Fig. 2b – Goldsmith et al., 2003). The complex tectonic of the Upper Triassic–Jurassic North Sea trilete rift system that led to the development of the border faults of the Viking Graben and Moray Firth half-grabens and grabens (Roberts et al., 1990; Ziegler, 1992), started with the post-rifting thermal subsidence of Upper Triassic–Lower Jurassic period (Ziegler, 1992; Steel, 1993) that was followed by a non-deposition or erosion of the lower-middle Jurassic deposits in the NNS during the Mid-Cimmerian Unconformity (Steel, 1993; Underhill and Partington, 1993; Coward et al., 2003; Johnson et al., 2005). Conversely, these deposits are better preserved further south (e.g., Inner Moray Firth – Patruno et al., 2019) and are locally overlaid by thin veneer of upper Jurassic mudstones and sandstones layers (Patruno et al., 2019; Scisciani et al., 2021).

The inherited Jurassic paleo-reliefs were passively infilled by Cretaceous sediments (Fig. 2) mostly covering the older sequences with very thin Lower Cretaceous claystones and marlstones (Cromer Knoll Group – Davies et al., 1999), and the more widespread Upper Cretaceous limestone and marls (Chalk/Shetland Groups – Patruno and Reid, 2016; Patruno and Reid, 2017; Patruno et al., 2019). These deposits are confined mostly in the southern basin, where they form thick syn-rift wedges in the hangingwall block of Cretaceous normal faults (e.g., Witch Ground Graben, Moray Firth Basin). As a contrast, in the northern area (e.g., Dutch Bank Basin, East Shetland Platform) the Cretaceous succession is typically much thinner (Patruno et al., 2019).

The Cenozoic non-marine, deltaic and shallow-marine mudstone-sandstone cycles (Fig. 2b) onlap the underlying Mesozoic deposits and progressively thins towards the west, with Tertiary deltaic progradational clinoforms expanding their thickness eastwards due to a regional tilting phase (Fig. 2a). In the western sector, close to the Shetland and Orkney islands, these deposits are often erosively truncated at the seabed. These sequences are generally only weakly deformed and affected by gentle folds and inversion structures related to the Alpine deformation phase (Pegrum and Spencer, 1990; Glennie and Underhill, 1998).

3. Data and methods

3.1. Well data

Stratigraphic, lithological, compressional seismic velocity (Vp) and bulk density (ρ) data of the sedimentary units (Devonian to Quaternary in age) were inferred from well data analysis of joined wireline and composite logs. The information from the 43 wells used in this study (Fig. 1) were retrieved from the UK National Data Repository (NDR – NSTA, 2022). The well-correlation showed in Fig. 3 briefly highlights the stratigraphic setting, showing also how poorly the basement was investigated at the centre of the GESP area. Only one well (7/16–1) was drilled in the inner part of the East Shetland Platform, at the junction between the Dutch Bank Basin and East Fair Isle Basin. It penetrated a presumed Permian-Devonian red to red/brown sandstone succession. A thick (600–2200 m) Cenozoic succession at the GESP margin is overlaying thin older sediments (e.g., Wells 16/02b-1, 9/16–2). Moving to the southernmost Moray Firth Basin (e.g., Wells 13/11–1, 13/14–1) the thickness of the Cenozoic sediments reduces, while a thick Cretaceous (mostly Lower Cretaceous) sequence stands out reaching thicknesses >2000 m (Fig. 3). Conversely, the Dutch Bank intra-basin wells (e.g., Wells 14/04–1, 8/27a-1) reveal a Jurassic-Triassic sediments thickening (100–700 m). Paleocene-to-Recent deposits show an eastward-thickening trend, reaching maximum thicknesses in the easternmost part of the study area (Well 16/02b-1), while the thickness of the Lower Eocene deposits shows significant lateral variations across the study area (Fig. 3).

The seismic velocity data (Table 1) were retrieved from 26 wells (Fig. 1b) among the total selected wells. These data were used to tie the seismic time-to-depth conversion. Despite the boreholes carrying wide ranges of velocities pertaining to each unit (Table 1), to simplify the time-to-depth conversion procedure we chose to set one seismic velocity value for each unit. The chosen values represent the weighted average of the seismic velocities from check-shot measured in wells (Table 1). Considering the lithological similarities between the units, and bearing in mind the stratigraphical uncertainties as reported in the logs, we grouped the Paleocene, Lower Eocene and Eocene-to-Recent deposits in one single seismic unit by attributing the interval velocity of 1907 m s^{-1}. The same approach was used for the Carboniferous?-Upper Devonian? and Lower-middle Devonian units that were grouped in one seismic unit and depth-converted with the interval velocity of 4067 m s^{-1} (Table 1). The Mesozoic and Paleozoic layers were depth-converted using velocities in the 2675–4558 m s^{-1} range (Table 1). Due to paucity of direct data, we assumed a seismic velocity of 6000 m s^{-1} for the basement, whilst the sea-water layer was depth-converted with a seismic velocity

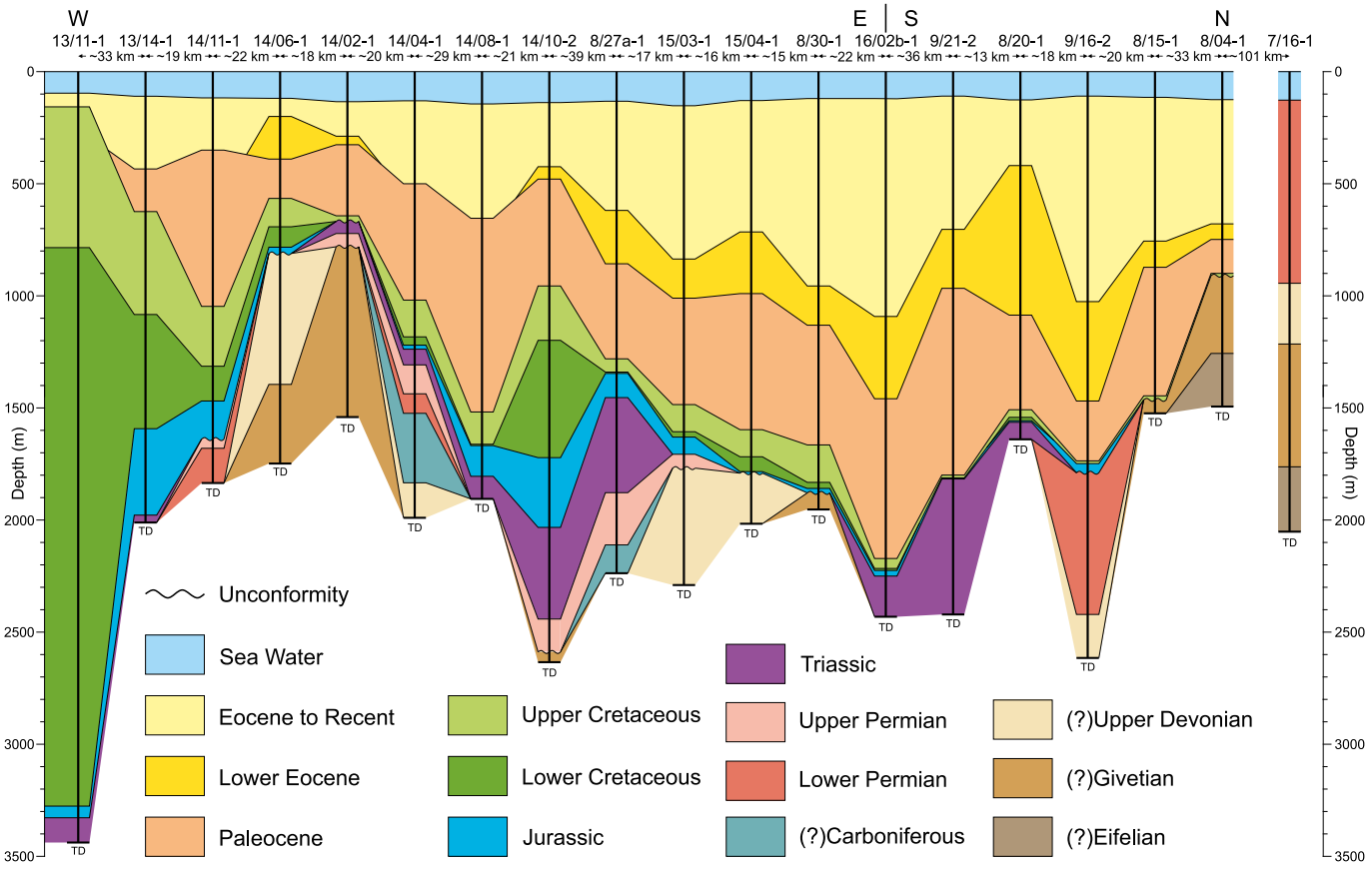

Fig. 3. Regional well-correlation panel (yellow line in Fig. 1). Well 7/16–1 was not correlated due to its distance (>100 km) from all the other wells. The lateral distance between the wells shown here is not to scale. (For interpretation of the references to colour in this figure legend, the reader is referred to the web version of this article.)

Table 1
Simplified stratigraphic column showing the layers and the relative values of seismic velocity, density and magnetic susceptibility adopted for time-to-depth conversion of seismic profiles and gravity and magnetic modelling.

Chronostratigraphy	Seismic Velocity ($m\ s^{-1}$)		Density (ρ, $kg\ m^{-3}$)		Susceptibility (k, SI)
Sea Water	1500[a]		1030[b]		-
Eocene to Recent (EtR)	1907	(1461 - 2253)	1997 - 2011	(1610 - 2156)	-
Lower Eocene (LE)			2021 - 2070	(1963 - 2129)	-
Paleocene (P)			2094	(1969 - 2240)	-
Upper Cretaceous (UK)	3725	(2399 - 5177)	2239 - 2550	(2239 - 2647)	-
Lower Cretaceous (LK)	3436	(2931 - 4397)	2232 - 2479	(1626 - 2571)	-
Jurassic (J)	2675	(1458 - 4705)	2072 - 2393	(2072 - 2451)	-
Triassic (T)	3515	(2813 - 4518)	2070 - 2385	(2070 - 2470)	-
Upper Permian (UP)	4526	(3192 - 5357)	2442 - 2587	(2428 - 2832)	-
Lower Permian (LP)	4558	(3859 - 5765)	2428 - 2558	(2292 - 2521)	-
Carboniferous? - Upper Devonian? (CuD)	4067	(3360 - 5460)	2335 - 2670	(2335 - 2670)	-
Lower-middle Devonian (emD)					
Basement (B)	6000[a]		2700 - 2750[b]		0.001 - 0.05[c]
Lower Crust (LC)	-		2900[b]		0.05[c]
Mantle (M)	-		3300[b]		0[d]

The values within brackets indicate minimum and maximum values retrieved from the available borehole data. Bold values were used for the depth-conversion and modelling. Reference values from: ([a]) Kearey et al. (2002), Reynolds (2011); ([b]) Lyngsie and Thybo (2007), Gradmann et al. (2013), Baykiev et al. (2018), Fichler and Pastore (2022); ([c]) Fichler et al. (2011), Beamish et al. (2016); and ([d]) Wasilewski et al. (1979), Wasilewski and Mayhew (1992).

of 1500 m s^{-1} (Kearey et al., 2002; Reynolds, 2011).

The modelling of the observed gravity anomalies was derived from the mean density (ρ) of each chronostratigraphic layer calculated from wireline bulk density logs (Table 1) available from 25 wells within and around the study area (Fig. 1b).

Relatively lower density values have been found in the Tertiary units (1997–2094 kg m^{-3}), while higher densities have been observed in the Upper Cretaceous (2239–2550 kg m^{-3}), followed downwards by lower densities in the Lower Cretaceous (2232–2479 kg m^{-3}), Jurassic (2072–2393 kg m^{-3}) and Triassic units (2070–2385 kg m^{-3}). The deeper intervals (Permian to Lower Devonian) show the highest densities (2335–2670 kg m^{-3}) within the sedimentary cover. In some cases, the synthetic blocks representing the same sedimentary unit were modelled with slightly different density values. These values always fall within the ranges provided by all well data (Table 1) but were contrained to the mearby well when available, hence the slight misfit. Reference density values were assigned to the sea water (1030 kg m^{-3}), basement (2700–2750 kg m^{-3}), lower crust (2900 kg m^{-3}) and mantle (3300 kg m^{-3}); these values are similar to those adopted in the surrounding areas (e.g., Lyngsie and Thybo, 2007; Gradmann et al., 2013; Baykiev et al., 2018; Fichler and Pastore, 2022).

3.2. Seismic data

The six lines investigated in this work (total line-length of about 1046 km), shown in Fig. 1b and described by PGS (2017) and Scisciani et al. (2021), have been selected from a 2D regional broadband seismic dataset covering the GESP (total line-length of about 15,000 km). This 2D survey was acquired and processed by PGS in 2016–2017 for the UK Oil & Gas Authority (OGA) (NSTA, 2017) and subsequently freely distributed to industry and academia via the NDR online platform (NSTA, 2022). In this work, we follow the Devonian-to-Recent GESP seismic-stratigraphic units grouping proposed in Scisciani et al. (2021).

These lines extend until 5 s two-way-time (TWT) depth highlighting a clear discrepancy between the shallow and deep reflectors. The Base Triassic-Top Upper Permian (Top Zechstein) reflector marks a distinctive change in the seismic facies with a high amplitude, laterally continuous bright trough. Above this, medium to high-amplitude laterally continuous reflectors can be observed. Directly beneath the Top Zechstein reflector, there are opaque low amplitude seismic facies until low-frequency high-amplitude zones are reached at depth.

The tectono-stratigraphic framework was defined by the interpretation of key horizons from the Sea Bottom to the Top Basement as reported in Table 1.

Starting from the seismic velocity values in Table 1, we depth-convert the six seismic lines using a simplified velocity model that provides an average value for each chronostratigraphic interval (Glover, 2000). The conversion function was guided by the following relationship (Etris et al., 2002):

$$Z = V_0 \frac{e^{kt} - 1}{k} \quad (1)$$

where Z is the thickness of the layers in meters, V_0 is the velocity at the top of the layer in m s^{-1}, κ corresponds to the variation frequency of the velocity with the increase in depth and t indicates the one-way time (t = TWT/2) for the layer thickness in seconds. Due to the extreme lateral variation of the seismic units and the resulting horizontal changes in seismic velocity with depth, a constant interval velocity model has been adopted to simplify the time-to-depth conversion. In this case, the κ parameter equals to zero and the previous relationship is simplified as follow:

$$Z = V_0\, t \quad (2)$$

3.3. Gravity and magnetic anomaly data

The gravity and magnetic anomaly data (Fig. 4) were acquired by Austin Exploration Inc. and were processed by Bridgeport Company (Bliss et al., 2016) that applied the following standard corrections to the original data (Bliss et al., 2016). The Bouguer gravity anomaly dataset was filtered with a 6 km cut-off Gaussian filter, interpolated on a regular 2 × 2 km grid and calculated with a reduction density of 1800 Kg m^{-3} (Fig. 4a). The magnetic anomaly data were interpolated on a 2 × 2 km grid, reduced to the pole (RTP) and filtered using a Gaussian filtering with an 8 km cut-off (Fig. 4b). The magnetic modelling was carried out using field data referred to the magnetic epoch of data acquisition (July–September 2016). In particular, the magnetic field intensity (*H*), inclination (*FI*) and declination (*FD*) were set to 40.475218 A/m, 72.121° and − 1.907°, respectively (Bliss et al., 2016).

Given the lack of borehole data concerning the magnetic susceptibility (k) of the modelled units, we modelled the magnetic anomaly data using k values within the range 0–0.05 SI units which is representative of the possible magnetic sources in the area (Telford et al., 1990; Lyngsie and Thybo, 2007; Fichler et al., 2011; Beamish et al., 2016). Within this range, lowest or null k values were attributed to the sedimentary units while higher values were used to model the basement and lower crust sources.

The modelling was constrained by the available literature also concerning the thermal gradients of the sedimentary and continental crust, and the depth of the Moho discontinuity. In particular, we model a thermal gradient of 30 °C km^{-1} for the sedimentary layers (Harper, 1971), and of 12 °C km^{-1} for the continental crust (Fichler et al., 2011; Gradmann et al., 2013; Baykiev et al., 2018; Fichler and Pastore, 2022). Finally, we model the Moho discontinuity ranging between 28 and 35 km depth (Fichler and Hospers, 1990; Fichler et al., 2011; Frogtech Geoscience, 2017 and references therein; Baykiev et al., 2018). Considering all the above, and assuming a Curie temperature of 600 °C, the Curie depth would fall below the Moho discontinuity. Since the mantle is not contributing to the observed magnetic anomaly (e.g. Wasilewski et al., 1979; Wasilewski and Mayhew, 1992), we can expect magnetic contributions from the entire crust.

In the study area, the Moho discontinuity shows a general westward-deepening trend since it ranges between 28 km depth in the area close to the Viking Graben, to about 35 km beneath the Shetland Islands and the Moray Firth Basin, while in the central part it is estimated to range between 32 and 34 km (Fichler and Hospers, 1990; Fichler et al., 2011; Frogtech Geoscience, 2017; Baykiev et al., 2018).

All the data described above were integrated in the following 2D combined forward modelling of gravity and magnetic anomalies (e.g., Garland, 1951; Telford et al., 1990; Düzgit et al., 2006; Rybakov et al., 2011; Mancinelli et al., 2020; Mancinelli et al., 2022).

4. Results

4.1. Bouguer gravity and magnetic grid observations

A pronounced gravity minimum of −30 mGal is observed at the centre of the Bouguer gravity anomaly grid (Fig. 4a). This minimum is grossly *E*-W elongated, with a NW-SE turn at its westernmost termination, roughly approximating the shape of the Dutch Bank Basin. Furthermore, two less pronounced gravity minima, both considering their amplitude and extension, are found in the East Orkney Basin (still with an approximate E-W trend) and in the East Shetland Platform (roughly N-S trend). In the southwestern portion (quadrants 6, 12 and 13), there is an area of high gravity anomaly with values > + 30 mGal. This V-shaped positive anomaly locates along the Caithness Ridge and the Fair Isle Platform, with E-W and NE-SW elongations, respectively. In the other parts of the study area (quadrants 7, 8), the gravity anomaly shows values ranging between +10 and − 10 mGal with the only exceptions found in the northernmost area, where two circular positive

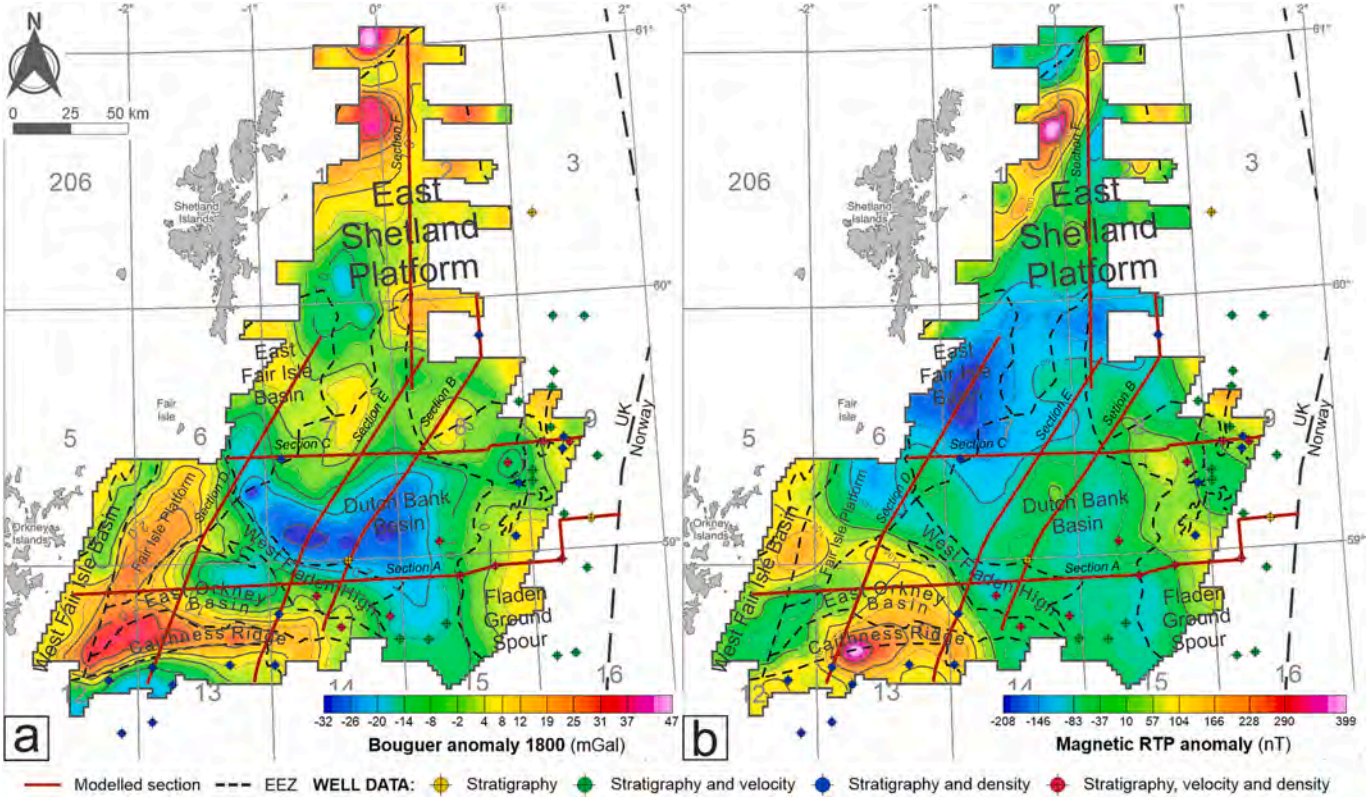

Fig. 4. Full anomaly grids (Bliss et al., 2016). (a) Bouguer gravity anomaly grid with a reduction density of 1800 kg m^{-3} and (b) reduced to the pole (RTP) magnetic anomaly grid. Both grids are 2 × 2 km spaced. Contour spacing is 5 mGal (1 mGal = 1 × 10^{-5} m s^{-2}) for (a) and it is 50 nT for (b). Black dashed lines indicate structural boundaries from Fig. 1. For any details about the standard corrections applied to these data, the reader may refer to Bliss et al. (2016). Wells labels are indicated in Fig. 1b. EEZ, exclusive economic zone; UK, United Kingdom.

gravity anomalies are partially covered by the dataset. Comparing the Bouguer gravity map and the interpreted seismic profiles, the anomaly highs generally match the areas of basement at shallow depth, while the lows are located over intra-platform Permo-Triassic basins (sensu Sciscciani et al., 2021).

The magnetic anomaly map (Fig. 4b) shows two notable peaks, a positive and a negative one. The ~ + 400 nT, 20 km-diameter positive peak is centred in quadrant 13, north of Wells 13/11–1 and 13/12–1 and east of the Section D. The magnetic anomaly minimum of ~ − 200 nT spatially relates with the East Fair Isle Basin. This minimum intercept the northern portion of the Section D and part of the Section C (Supplementary Figs. S1, S2) where the basement is shallow underneath a thin cover of Lower Permian to Lower Devonian sediments in the East Shetland Platform. In the south-eastern half of the study area, the magnetic anomaly shows wide undulations with anomaly values in the range + 30/−70 nT. In this area, a thick sedimentary cover is highlighted from the seismic profiles (supplementary fig. S5). In the northern sector of the study area, a positive-negative couplet is partially covered by the dataset.

As an additional constraint to the forward modelling, we calculated the time thickness map of the Mesozoic interval across the study area (Fig. 5). The overall distribution of this interval throughout the survey was derived from Sea Bottom, Base Tertiary (Top Chalk) and Base Triassic (Top Zechstein) reflectors. When compared with the contours of the Bouguer anomaly map in Fig. 4a, the resulting map shows how the spatial distribution of the maximum thicknesses of the Mesozoic succession closely correlates with the Bouguer gravity minima (Fig. 5).

Furthermore, to better understand the Bouguer gravity and magnetic anomalies correlations with structural features in the study area, we performed a simple filtering of the original datasets. In particular, using a 50 km wavelength threshold, we calculated high-pass (HP) and low-pass (LP) anomalies of both the gravity and the magnetic datasets (Fig. 6).

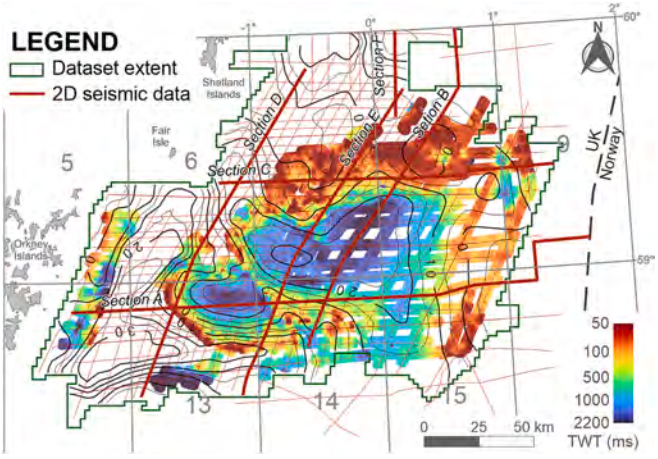

Fig. 5. Time thickness grid of the Mesozoic sequence. Black lines represent the contour of Bouguer gravity anomaly (contour interval 5 mGal) from Fig. 4a. Thin red lines are traces of the interpreted 2D seismic lines (NSTA, 2022) used to calculate the time thickness maps; thick red lines show the sections modelled in this work. Green line shows the extension of the Bouguer gravity and magnetic anomaly data from Bliss et al. (2016). (For interpretation of the references to colour in this figure legend, the reader is referred to the web version of this article.)

While the gravity signature of the Dutch Bank Basin is removed by the HP filter (Fig. 6a), in the southwestern area, the HP gravity anomaly highlights further features with a more limited extension (small <50

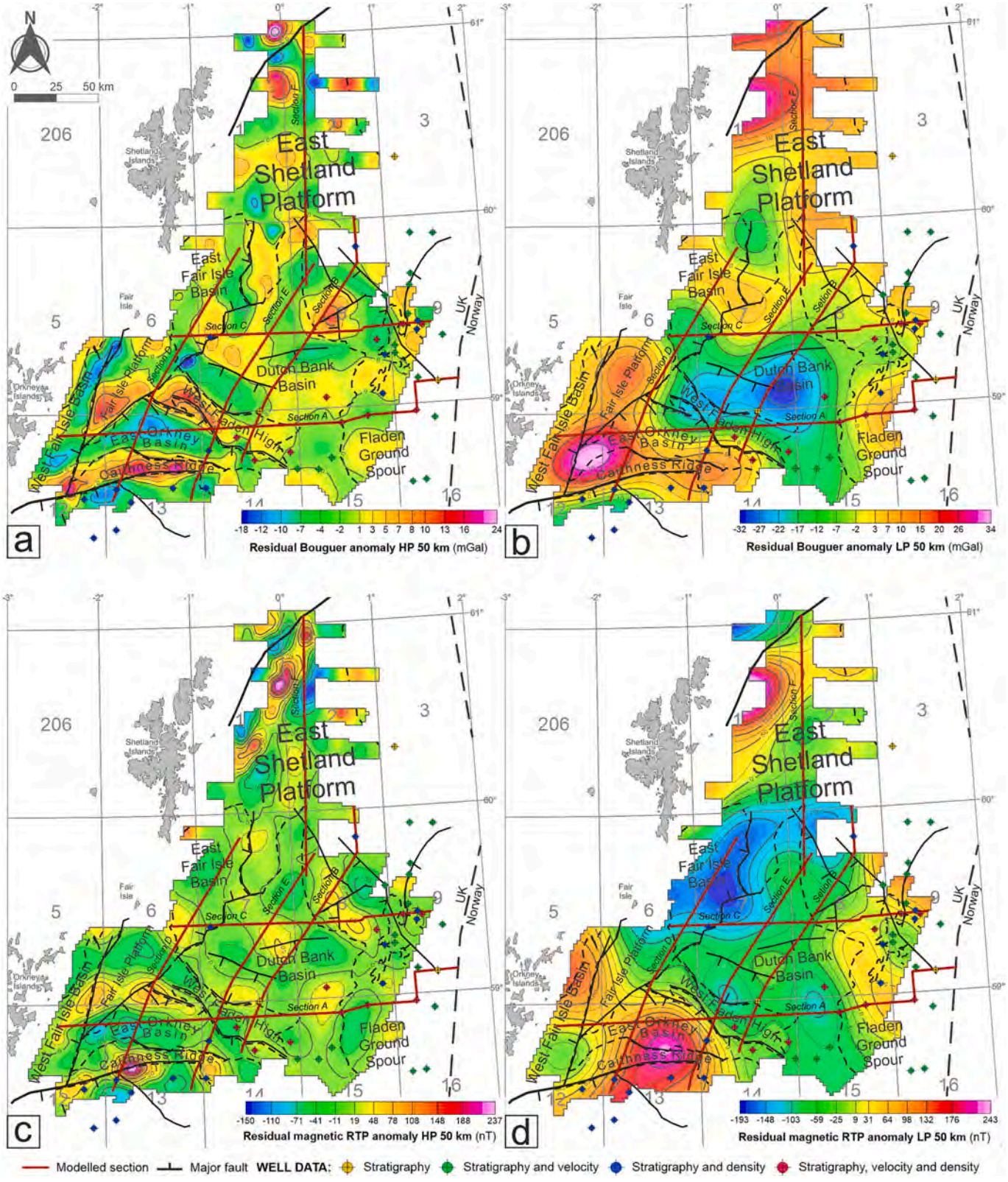

Fig. 6. Filtered gravity and magnetic datasets. (a) 50 km high-pass (HP) Bouguer gravity. (b) 50 km low-pass (LP) Bouguer gravity. (c) 50 km HP magnetic anomaly. (d) 50 km LP magnetic anomaly. Contour spacing is 5 mGal for (a) and (b) and it is 25 nT for (c) and (d). Structural elements modified from Scisciani et al. (2021). Black dashed lines indicate structural boundaries from Fig. 1. See Fig. 1b for well and seismic lines labels.

km), clearly matching with local basement highs and basins delimited by major faults (e.g., Scisciani et al., 2021). The sedimentary basins (e.g., East Orkney Basin, West Fair Isle Basin) almost retrace the gravity lows, as well as the basement highs (e.g., Caithness Ridge, West Fladen High, Fair Isle Platform) are matched by gravity highs. On the contrary, the LP Bouguer anomaly (Fig. 6b) enhances the E-W gravity minimum found in the Dutch Bank Basin and the positive signature in the western sector of the Caithness Ridge. These two gravity signatures are clearly related to wide and/or deep sources carrying strong negative and positive density contrasts, respectively.

The same filtering process was applied to the RTP magnetic anomaly grid. In comparison with the full anomaly map in Fig. 4b, the HP magnetic anomaly (Fig. 6c) shows a general ±50 nT trend throughout the study area with local exceptions found on the Caithness Ridge and in the northernmost part of the dataset, where the E-W negative-positive-negative trend persists, suggesting low-wavelength sources. A local ~ − 100 nT minimum is observed in the westernmost part of the East Orkney Basin, surrounded by local maxima southwards (Caithness Ridge), to the northeast and to the northwest (towards the West Fair Isle Basin). The LP magnetic anomaly shown in Fig. 5d, depicts a wide minimum (~ − 200 nT) in the East Fair Isle Basin and a near-circular maximum (~ + 250 nT) on the Caithness Ridge.

The full anomaly maps and the low- and high-wavelength components of the gravity and magnetic anomalies show significant spatial correlations with the main tectonic features throughout the study area (Figs. 4, 5 and 6). This is sufficient motivation to further investigate the observed anomalies and address their sources by forward modelling the geometries retrieved after the time-to-depth conversion of the seismic data against the observed full Bouguer gravity and magnetic anomalies. For the sake of brevity, in the following chapter we discuss only two of the six modelled sections. These two sections, namely Section A and Section B, carry results that are representative also for the other four sections that are showed in the supplementary material (Supplementary Figs. S1-S4).

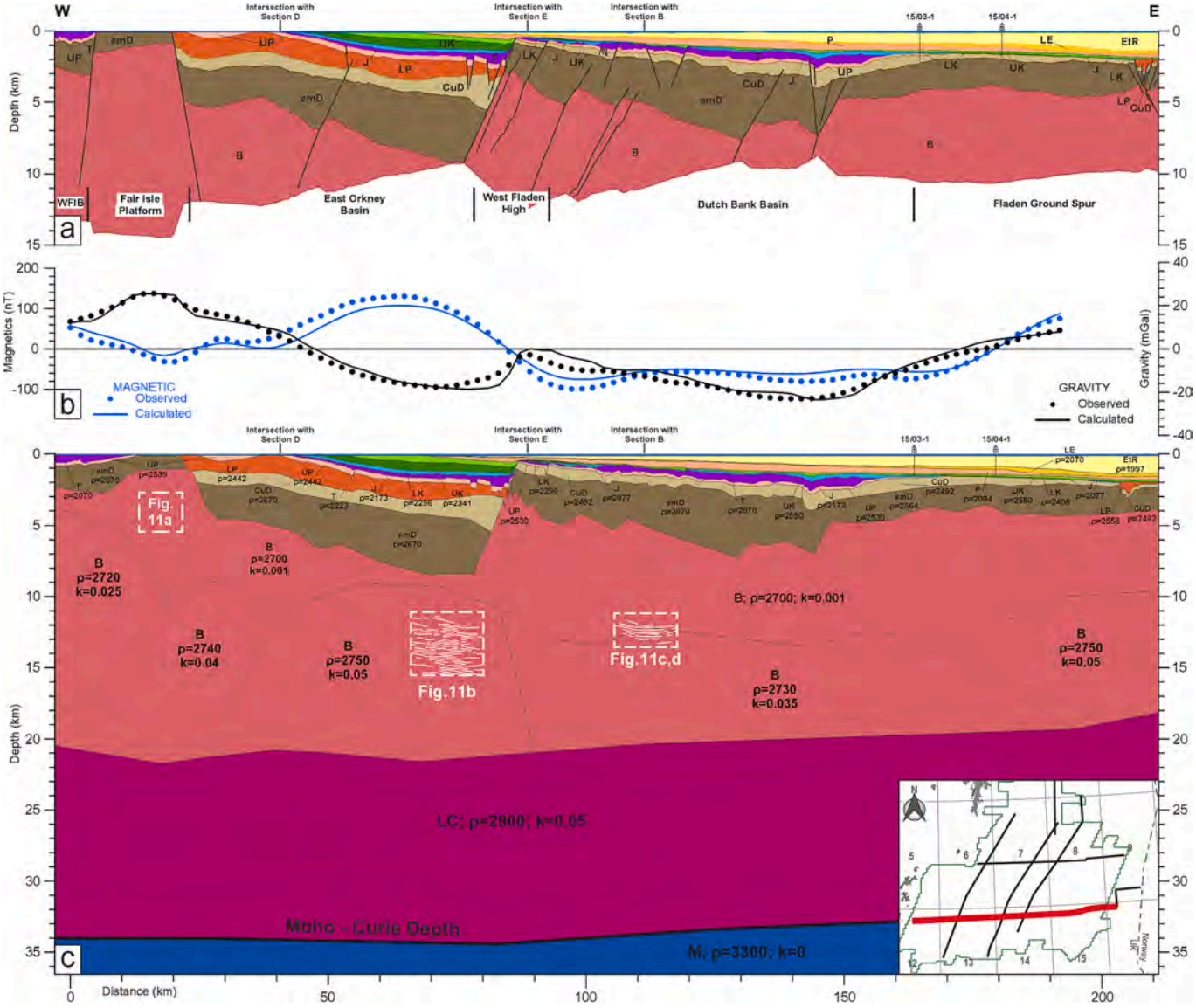

Fig. 7. Gravity and magnetic anomalies model across the Section A. (a) Depth-converted section. (b) Anomaly curves best fitting. (c) 2D integrated forward model. Modelled density (ρ) and magnetic susceptibility (k) values are given for each block in the lower panel. Bathymetry across the modelled profile ranges between 50 and 150 m. Colours and label abbreviations are the same of those shown in Table 1. In the inset, the thick red line shows the extent of the modelled section while the green line represents the extent of the modelled gravity and magnetic anomaly grids. White dashed boxes locate seismic reflections (white thin continuous lines) shown in Fig. 11. WFIB, West Fair Isle Basin. (For interpretation of the references to colour in this figure legend, the reader is referred to the web version of this article.)

Density and magnetic susceptibility values used in the modelling procedure have been kept in the ranges reported in Table 1 (bold values) across all the modelled sections. It should be noted that all the values used for the modelling fall within values retrieved from the available wellbores (bold and within-brackets values in Table 1). The modelling was constrained by cross tie between the sections; in particular, each modelling step was performed by minimizing the misfit between crossing sections both considering the depth of the modelled horizons and the densities and magnetic susceptibilities of the modelled blocks. The following chapter illustrates the resulting best-fit models.

Below the depth-converted seismic data, the geometries of the synthetic blocks proposed in the resulting models (Figs. 7, 8 and S1-S4), are constrained only to the coinciding Curie and Moho depths and to the observed gravity and magnetic anomalies, no other interpretative constraint is included.

4.2. Modelling results

Fig. 7 shows the depth-converted (Fig. 7a) and the modelled (Fig. 7c) Section A. In the eastern sector of the East Orkney Basin, in the hanging-wall of the main boundary normal fault, the depth-conversion results in ~9000 m of sedimentary sequence with significant contributions from the Carboniferous?-to-Lower Devonian (4000–6000 m in thickness), Lower Permian (1000–2000 m in thickness) and Cretaceous (1000–1500 m in thickness) deposits, respectively. Another main sedimentary depocenter is located in the Dutch Bank Basin where, conversely to what found in the East Orkney Basin, the Cretaceous and Permian sequences are extremely thin or completely missing. Along the section, Palocene-to-recent deposits are absent in the western sector, and they increase in thickness east of the East Orkney Basin towards the maximum thickness of ~2000 m. The modelled depth of the basement

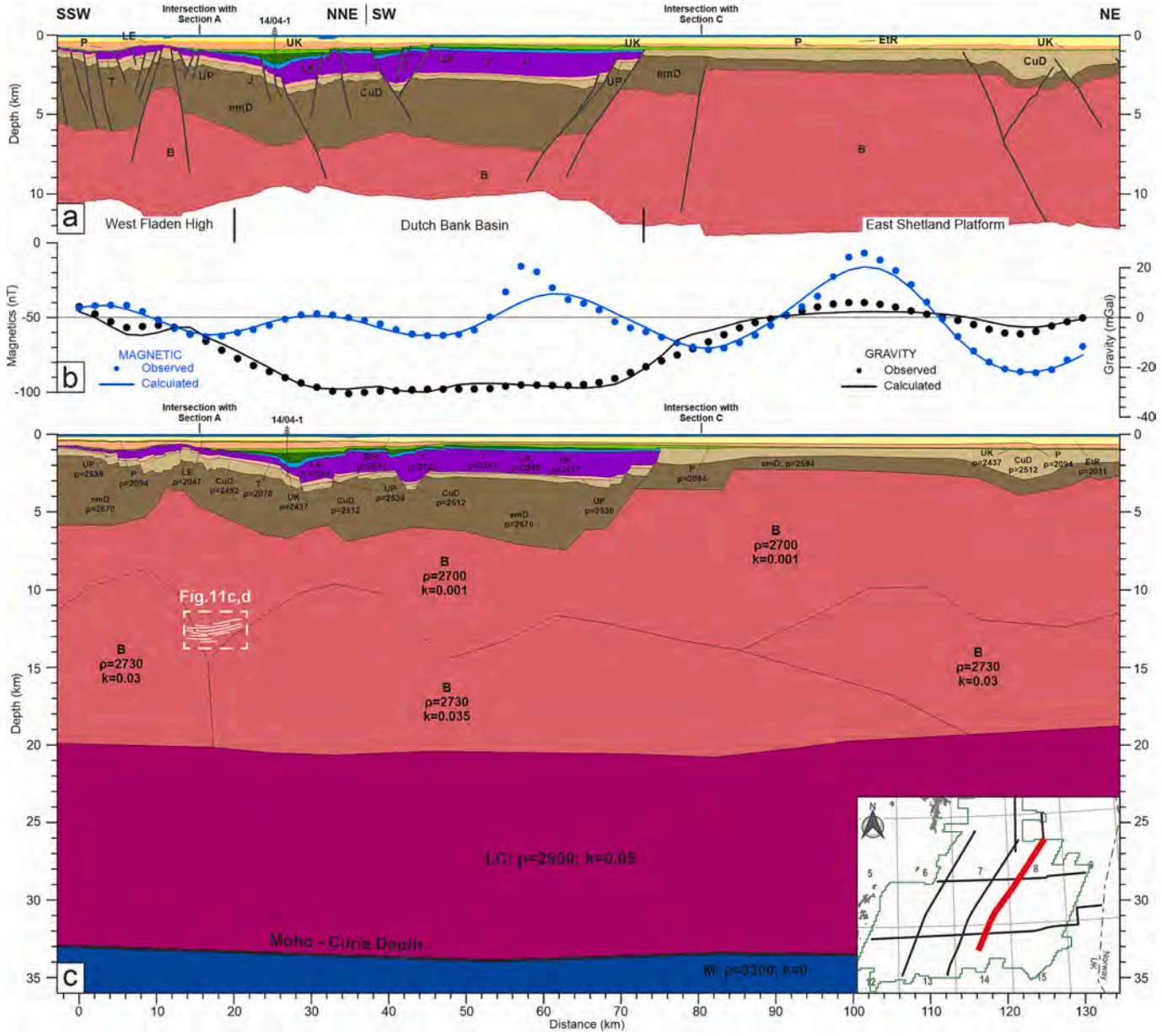

Fig. 8. Gravity and magnetic anomalies model across the Section B. (a) Depth-converted section. (b) Anomaly curve best fitting. (c) 2D integrated forward model. Modelled density (ρ) and magnetic susceptibility (k) values are given for each block in the lower panel. Bathymetry across the modelled profile ranges between 50 and 150 m. White dashed boxes locate seismic reflections (white thin continuous lines) shown in Fig. 11. Colours and label abbreviations are the same of those shown in Table 1. In the inset, the thick red line shows the extent of the modelled section while the green line represents the extent of the modelled gravity and magnetic anomaly grids. (For interpretation of the references to colour in this figure legend, the reader is referred to the web version of this article.)

along section A is ~1500 m shallower in the western side of the East Orkney Basin (hangingwall block to the east of the Fair Isle Platform).

The modelling results of the observed Bouguer gravity and magnetic anomalies, being constrained by well and literature data, are consistent with the geometries of main crustal blocks retrieved after the depth conversion. This is demonstrated by the good fit obtained both in the Bouguer gravity and magnetic anomaly profiles (Fig. 7b) with maximum mismatches of ±5 mGal and ± 15 nT, respectively. Interestingly, the gravity and magnetic anomalies show divergent trends from the West Fair Isle Basin to the westernmost end of the Dutch Bank Basin. In the East Orkney Basin, the gravity reaches its minimum due to the thick sedimentary cover infill, and the magnetic reaches its maximum in the central part of the basin (Fig. 7b). Considering the null magnetic contribution carried by the sedimentary cover, we model the lower crust and the basementwith high magnetic susceptibilities (0.05 and 0.025–0.05 SI units, respectively) suggesting strong magnetic composition of the basement both beneath the East Orkney Basin and the Dutch Bank Basin.

Across this section, the top of the lower crust ranges between 18 and 22 km with a gentle westward-deepening trend, while the Curie depth, coinciding with the Moho discontinuity, ranges between 32 and 35 km..

Fig. 8 shows the depth-converted (Fig. 8a) and the modelled (Fig. 8c) Section B. In the Dutch Bank Basin the depth-conversion results in ~7000 m of sedimentary sequence still with the significant contribution from the Carboniferous-to-Lower Devonian deposits (4000–5000 m thickness). Furthermore, the thickness of the Triassic sediments increases from the West Fladen High (500 m) to the Dutch Bank Basin (1500–2000 m) while in the East Shetland Platform these intervals are lacking. On the contrary, the sedimentary cover tends to thin in the northern half of this section where the basement reaches its shallowest depth (2000–2200 m).

A good fit was obtained both in the gravity (±6 mGal) and magnetic (±16 nT) profiles (Fig. 8b). Compared to the Section A, the gravity and magnetic anomalies along the Section B shows divergent trends from the Dutch Bank Basin to the westernmost end of the GESP. In fact, in this section the gravity anomaly reaches its minimum where the maximum thickness of the Triassic sediments is found in the Dutch Bank Basin. On the contrary, the magnetic anomaly shows wide fluctuations reaching local maxima both in the Dutch Bank Basin and in the East Shetland Platform (Fig. 8b). As in the previous section, also in this case we model both the basement and the lower crust with high magnetic susceptibilities (≥0.03 SI units) suggesting strong magnetic contributions of the basement beneath the Dutch Bank Basin.

Across this section, the top of the lower crust is found at ~19–20 km, while the Moho-Curie depth ranges between 32.5 km depth at the southernmost and northernmost ends of the section, and 34 km depth in the central part of the section, beneath the Dutch Bank Basin.

Comparing the best-fitting geometries across the modelled sections with the depth-converted interpretations of the seismic lines we find a general good match of such interpretations with the modelled synthetic blocks.

Considering that the results presented above are representative for all the modelled sections we can draw some general considerations about the spatial relations between the modelled Bouguer gravity and magnetic anomalies and their main sources.

Lower-Devonian to Carboniferous sequences show significant thickness (1000–5000 m) throughout the study area with four main depocenters striking W-E to NW-SE, two located in the southern part (i.e. East Orkney Basin and Dutch Bank Basin) and two in the northern part (i.e. East Fair Isle Basin, East Shetland Platform) of the study area. In the southern basins we find the higher thicknesses (>3000 m), while in the northern basin we find the thinnest Devonian-Carboniferous sequences (<3000 m). Despite their lateral variations of thickness, these unit do not spatially relate to the observed Bouguer gravity anomaly. In fact, in the modelled sections, the thickening of these sequences is not ubiquitously matched by a local minimum of the Bouguer anomaly (e.g. the southernmost end of section B in Fig. 8), while the thinning of these deposits does not always corresponds to local Bouguer anomaly maximum (e.g. between km 90 and 140 of section C in Fig. S1). Furthermore, local Bouguer anomaly undulations are not matched by significant thickness changes of the Devonian-Carboniferous sequences (e.g. between km 30 and 100 of section E in Fig. S3).

The Lower Permian units are found only in the western part of the study area (i.e. East Orkney Basin and East Fair Isle Basin) with maximum thickness of ~1500 m (Fig. 7, supplementary Fig. S1, S2) while they are lacking in the northern part of the study area (i.e. Dutch Bank Basin, East Shetland Platform, West Fladen High; Fig. 8, supplementary Fig. S1, S3). This asymmetrical distribution reflects the non-deposition or erosion of this interval in the Dutch Bank Basin, West Fladen High and East Shetland Platform due to the Lower Permian uplift affecting these areas (Patruno et al., 2019; Scisciani et al., 2019). Furthermore, this uplifting resulted in the deposition of less than 200 m thickness of Upper Permian sequence that extends mostly from the easternmost Dutch Bank Basin to the westernmost East Orkney Basin, and in the West Fair Isle Basin (Fig. 7). In fact, in this area the Upper Permian deposits are present only in the Crawford-skipper Basin (Fig. S1) where the complex structural framework allowed also Lower Permian deposition. Across this sedimentary basin, the geometries resulting from the seismic interpretation of Scisciani et al. (2021) properly fit the modelled gravity anomaly (Fig. S1).

The development of *syn*-tectonic intra-platform extensional basins and the later rifting tectonic phase (Roberts et al., 1990; Ziegler, 1992; Steel, 1993; Underhill and Partington, 1993; Coward et al., 2003; Johnson et al., 2005; Phillips et al., 2019), has driven the distribution of Triassic deposits (Patruno et al., 2019; Scisciani et al., 2021). Section A (Fig. 7) shows quite constant *E*-W thickness of this unit. Instead, the N-S spatial distribution of this interval is better highlighted in Section B (Fig. 8) where a north-eastward thickening, from 700 to 2000 m is observable. Triassic unit are thinner southwards moving from the basins (e.g., Dutch Bank Basin) to the nearest structural highs (e.g., West Fladen High) while these deposits are completely lacking in the northern area (e.g., East Shetland Platform).

The thickness of the Jurassic deposits is moderate (200–300 m) throughout the study area. In Fig. 7, a thin Jurassic layer is visible. It extends from the westernmost East Orkney Basin to the easternmost Dutch Bank Basin, conformably overlying the Triassic sequence. On the contrary, looking at the N-S profiles (Fig. 7, S3) its thickness (200–300 m) tends to decrease eastward whilst in the N-S direction it maintains a constant thickness. The modelling of the Bouguer gravity anomaly highlights how the distribution of the Triassic-Jurassic deposits matches with the main gravity low in the Dutch Bank Basin (Fig. 9c). This is observed throughout all the sections crossing the latter (Figs. 7, 8, supplementary Fig. S3) where a drop of the gravity anomaly appears over the maximum Triassic thickness.

The Lower Cretaceous E-W trend shows a constant thickness (<250 m) enclosed in the East Orkney Basin, where the deposits infilled the tilted paleo-reliefs. Where present, in the remaining of the southern area (e.g., Dutch Bank Basin), it allocates a thin layer (<100 m thickness), while in the north (e.g., East Shetland Platform, East Fair Isle Basin) it is completely missing. N-S trend of Lower Cretaceous unit highlights that this deposit is limited to the principal basins (e.g., East Orkney Basin, Dutch Bank Basin) with maximum thicknesses found at their centres. Similarly, Upper Cretaceous deposits are found as really thin (<200 m) layers, but they are spatially widespread (Figs. 7, 8, 9a, Supplementary Fig. S1, S3).

The thickness of the Paleocene-to-Recent units presents a constant N-S trend but it tends to increase eastwards, towards the Viking Graben (up to 2000–2500 m; Fig. 7, supplementary Fig. S1). On the contrary, this unit is completely missing in the western sector of the study area (quadrants 5, 6, 12 and 13) and its spatial distribution does not match the trends of the Bouguer gravity anomaly across the modelled sections (e.g., Figs. 7, 8).

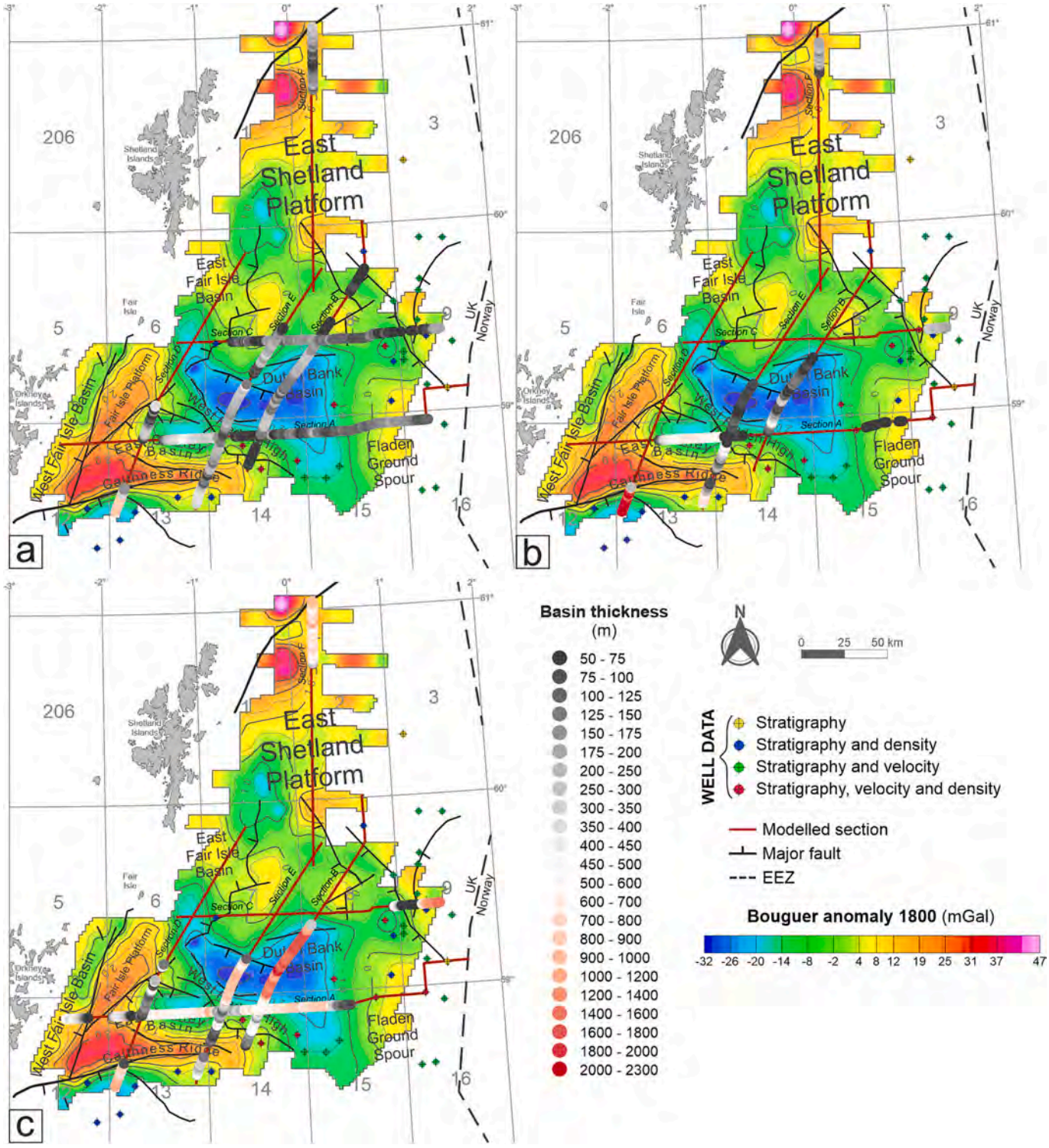

Fig. 9. Thickness values of (a) Upper Cretaceous, (b) Lower Cretaceous and (c) Triassic-Jurassic deposits overlying the Bouguer gravity anomaly map. Parts of the profile where dots are missing represent deposits with thickness < 50 m, representing erosion or non-deposition. Thickness of the mapped deposits are all shown with the same black-red colour scale. Structural elements modified from Scisciani et al. (2021). Labels of the main structural features correspond to those in Figs. 1, 4 and 6. See Fig. 1b for well labels. EEZ, exclusive economic zone; UK, United Kingdom. (For interpretation of the references to colour in this figure legend, the reader is referred to the web version of this article.)

Across the entire study area, we found a close spatial relationship between the distribution of Bouguer anomaly lows and the depocenters of sedimentary basins. This can be clearly seen in the East Orkney Basin and in the Dutch Bank Basin – i.e. the two main depocenters of the study area (Figs. 7, 8). Conversely, the gravity anomaly tends to reach high values where the thickness of the sedimentary deposits is reduced. The main gravity minimum (Fig. 4a) is located above the Triassic depocenter in the Dutch Bank Basin (Fig. 7b, 8b, supplementary Fig. S3), whilst the extent of the East Orkney Basin gravity minimum matches the Lower Cretaceous deposits extension (e.g., Fig. 7). This evidence is further

clarified in Fig. 5 where the correspondence between the maximum thickness in time and the contour of the gravity anomaly is observable. Long-wavelength undulations (≥100 km) of the Bouguer gravity anomaly are mostly controlled by the depth to the top-basement. However, low-density contributions from sedimentary basins are always required in order to fit the observed long-wavelength gravity anomalies (Figs. 7, 8, supplementary Fig. S1-S4).

Concerning the sources for the modelled magnetic anomaly, we locate three distinct sets, each contributing in function of their thickness, depth and lateral extent. The shallow sources, roughly corresponding with the upper portion of the basement were modelled with an average susceptibility value of 0.001 SI units, the deepest sources are found in the lower crust and they are modelled with magnetic susceptibility of 0.05 SI units. Finally, the central sources are found at intermediate depths (i.e. in the middle crust, beneath the upper basement and the lower crust) and they were modelled with lateral variations of magnetic susceptibilities ranging between 0.02 and 0.05 SI units, corresponding to density values ranging between 2720 and 2750 Kg m^{-3}, respectively. As expected, the magnetic contribution of the Devonian-to-Tertiary sedimentary sequences is null (i.e. magnetic susceptibility is zero) due to their sedimentary nature.

5. Discussion

Historical uncertainties about the under-explored GESP led us to investigate the structural framework of this area by a detailed and multidisciplinary approach supported by recent high-quality data. Bearing in mind the non-uniqueness of the potential field modelling, all the available constraints were included to evaluate the gravity and magnetic contributions against the observed anomalies. Such approach was further encouraged by the spatial correlation we found between the high- and low-wavelengths components of the modelled anomalies and well-known tectonic features across the study area (Fig. 6).

Geometrical models retrieved after the time-to-depth conversion of the seismic interpretations required little adjustments once their gravity and magnetic signature were modelled. Maximum vertical shifts ≈500 m was required for the geometry of the Lower-middle Devonian and top of the Caledonian basement in section B (e.g., in the Fair Isle Platform – Fig. 7) in order to fit the observed gravity and magnetic anomalies. For all the other sections the vertical shift was <300 m. Considering the uncertainties derived from the seismic data interpretation and time-to-depth conversion, this is not surprising. Other minor adjustments were required, in order to fit the observed gravity and magnetic anomalies, concerning the shape and dip of major faults affecting the basement. Similarly, the intersections between crossing modelled sections were used as control-points for the correctness and coherency of the models both for geometries and properties of the modelled blocks. The models shown in Figs. 7, 8 and Supplementary Figs. S1-S4 were achieved with maximum misfit at intersections of 100 kg m^{-3} and 0 (SI units) concerning the density and the magnetic susceptibility of the Devonian-to-recent sedimentary units, respectively. The misfit concerning the density values is always bounded to the ranges provided in Table 1, with local well data driving local variations of densities. In other words, the density values that were used to model a section derive from the closest well, resulting in a maximum 100 kg m^{-3} misfit at intersections. Concerning the basement, lower crust and mantle blocks the models were achieved with zero misfit both concerning the density and magnetic susceptibility of the synthetic blocks and with maximum misfit of tens of meters concerning the depth of the modelled horizons (i.e. block boundaries).

Considering that the modelling has benefited from all the geological and geophysical constraints available in public data repositories or in the published literature, we provide a detailed and geologically-consistent reconstruction of the crustal geometries in the GESP that expands the discussion already proposed by previous authors (e.g., Fichler and Hospers, 1990; Holliger and Klemperer, 1989; Holliger and Klemperer, 1990; Fichler et al., 2011; Kimbell and Williamson, 2016; Frogtech Geoscience, 2017).

Interestingly, the gravity and magnetic anomalies, both considering their full (Fig. 4) or filtered (Fig. 5) signatures, do not relate to each-other and often show opposite trends (Figs. 7, 8, supplementary Fig. S1-S4). We interpret this evidence as a differentiation of sources for the two modelled fields. In fact, commonly the trend of the top of basement governs both the magnetic (being the first contributor with depth) and the gravity anomaly (being the first ubiquitous density contrast), but this is not the case in the GESP. On one side we found high-susceptibility bodies (up to 0.05 SI units) throughout the modelled sections, these sources control the magnetic signature. While on the other side, we report strong contributions due to Mesozoic sedimentary sequences in the main basins especially Triassic and Cretaceous intervals (i.e. Dutch Bank Basin, East Orkney Basin) that alter the gravity signature at different wavelengths, corresponding to the size of the source basin. Following previous authors, we do not consider remanent magnetization but limit the modelling to induced contributions (e.g., Fichler et al., 2011).

We split the following discussion in two main parts, one concerning the outcomes of the gravity modelling and one concerning those related to the magnetic modelling.

5.1. Gravity modelling outcomes

Three main intervals were distinguished by the interpretation of seismic profiles and their thicknesses were reconstructed (Fig. 9). Based on well-to-seismic ties, they correspond to the Upper Cretaceous (Fig. 9a), Lower Cretaceous (Fig. 9b) and Triassic-Jurassic (Fig. 9c), and they are indicative of three different tectono-sedimentary phases in the evolution of the GESP (Fig. 2b).

It is evident that the Triassic and Jurassic deposits mainly contributed to the Dutch Bank Basin infill, while the Cretaceous deposits mostly contributed to the East Orkney Basin and Moray Firth Basin, south of the Caithness Ridge. The thickness trend of the Triassic deposits in the Dutch Bank Basin (e.g., Figs. 8, 9) exhibits evident decrease both southwards and eastwards with values <800 m. Instead, thicknesses of 1500–2000 m (Figs. 8, 9) are mainly found in the depocenter where the minimum in low-pass filtered anomaly is found (Fig. 6b).

The East Orkney Basin is surrounded by gravity highs (Figs. 5, 6, 9). The Lower Cretaceous deposits in this basin are clearly affected by major faults (Figs. 5, 6, 9b) contributing, with the Jurassic and Triassic layers (Fig. 9c), to the observed Bouguer anomaly low.

Such observations suggest a differential tectonic control through the GESP during the Triassic-to-Cretaceous times. The Dutch Bank Basin was the main depocenter during the Triassic-Jurassic times, with a reduced sedimentary input in Cretaceous times. On the contrary, the East Orkney Basin showed a reduced sedimentation rate in the Triassic-Jurassic times and relatively high subsidence during the subsequent Cretaceous phase. The full (Fig. 4a) and filtered (Fig. 5a and b) gravity maps support a dimensional relationship between the basins and the gravity anomaly.

The thickness of the Triassic and subordinately of Jurassic mudstones/sandstones deposits in the Dutch Bank Basin show evident lateral variations, with maximum values of ~2000 m (Figs. 7, 9a) found in the central and northern part of the basin in the hangingwall block of a set of SS*E*-dipping normal faults, and decreasing both westwards and southwards within the basin. The density used to model this unit (2070–2393 kg m^{-3}) is compatible with mudstones/sandstones and valid across the entire basin. The north-eastward thickening across the latter (Fig. 8, supplementary Fig. S3) and the abrupt northern termination against the WSW-ENE to WNW-ESE trending normal faults, in addition to the spatial distribution of the gravity depocenter, suggests a faulting mechanism related to grossly N-S to NW-SE oriented extensional axis. Faults with similar attitude and with Triassic and probably pre-Triassic *syn*-tectonic growth wedges have been also described in the East Shetland Basin and Unst Basin (Claringbould et al., 2017). This suggests that the overall GESP probably suffered an early N-S trending extension culminated in

Triassic times and subsequently, during late Jurassic and Cretaceous, underwent near E-W to NE-SW trending extension. This second phase was preceded by a regional uplift (Late Cimmerian inversion in Patruno et al., 2019) and subsequently produced a marked footwall uplift along the main faults bounding the major basins (e.g., the Fladen Ground Spur along the western margin of the Viking Graben and the West Fladen High along the eastern margin of the East Orkney Basin). The concomitant uplift occurred along the eastern and south-western part of the Dutch Bank Basin prevented the erosion of the pre-Jurassic succession, only at the central part of the basin where the Triassic depocenter has been preserved. This two-stage evolution promoted the development of an approximately E-W trending Mesozoic basin with a distinctive shape and dissimilar from trends of other basins across the GESP area. At regional scale, the Dutch Bank Basin represents the lowest gravity anomaly within the entire GESP area with a clear E-W elongation, in contrast with the N-S trend of previously reconstructed Triassic basins especially along the Norwegian continental platform located to the east of the Viking Graben (e.g., Steel and Ryseth, 1990; Nøttvedt et al., 1995; Færseth, 1996; Richardson et al., 2005; Bell et al., 2014; Phillips et al., 2019). Once the gravity grid is filtered with 50 km high-pass and low-pass cut-off (Fig. 6a, b), it preserves its E-W shape only on the low-pass output (Fig. 6b), still locating the lowest observed gravity anomaly within the study area.

An impressive correlation between tectonic elements and gravity anomalies is find in the south-western area on the high-pass filtering (Fig. 6a). The match between the structural framework and the gravity anomaly is enhanced by this filtered grid, allowing to infer the gross extent of these tectonic structures at different scales of view. Additionally, small depocenters (supplementary fig. S6) (i.e. north of West Fladen High, northeast of East Fair Isle Basin, southern part of West Fair Isle Basin), that were not directly crossed by the modelling but are visible in the seismic sections, stand out in the filtered grid. Considering the gravity footprints of the latter, and supported by the outcropping Cretaceous deposits reported by the offshore bedrock map (BGS, 2022), we suggest that these were filled by Mesozoic (i.e. Lower Cretaceous, Jurassic, Triassic) sediments as well. This interpretation is supported by the comparison with the gravity signatures generated by the aforementioned Triassic and Cretaceous units (Figs. 4a, 6a) and observed in the modelling of section A (Fig. 7).

The main contributions to gravity lows are provided by the Cretaceous, Jurassic and Triassic deposits. The underlaying Permian and Devonian successions, due to their relative basement-like high-density, have a minor influence on gravity anomaly distribution with respect to the younger sediments. Consequently, the gravimetric modelling results particularly useful to distinguish between Mesozoic and Paleozoic basins. This is very significant for the study of basins occurring at shallow depths close to the Shetland and Orkney Islands, where seismic show reflective intervals overlaying the basement but the absence of well control prevents to define the age of these basins.

5.2. Magnetic modelling outcomes

The comparison between the main structural elements (Fig. 1b) and the full (Fig. 4b) or filtered (Fig. 6c, d) magnetic anomaly maps does not highlight any evident correlations between the fault-controlled basins and mapped anomalies. Considering the sedimentary nature of the post-Caledonian units (Fig. 2), possible magnetic sources are located within the basement and lower-crust (e.g., Donato and Tully, 1982; Holloway et al., 1991; Bassett, 2003; Fichler et al., 2011; Patruno et al., 2017; Scisciani et al., 2019; Kombrink and Patruno, 2020).

In our interpretation, the shallower portion of the basement, mainly composed of metamorphosed sediments (Bassett, 2003; Patruno et al., 2017; Scisciani et al., 2019; Kombrink and Patruno, 2020), contributes with low-susceptibility values (0.001 SI units) while deeper contributions are related to high-susceptibility bodies. This is also consistent with previous studies where high-susceptibility bodies were inferred within the crust (Donato and Tully, 1982; Fichler et al., 2011; Beamish et al., 2016; Arsenikos et al., 2018).

As stated before, the parametrization of the modelled blocks was carried out considering all the available geological constraints. Among these we include information of metamorphic and igneous facies from exposures and boreholes in and around the study area (Fig. 10; Bassett, 2003; Fichler et al., 2011; Patruno et al., 2017; Scisciani et al., 2019; Kombrink and Patruno, 2020; BGS, 2022).

Some high susceptibility body values (0.025–0.05 SI units) at 15 km depth were modelled throughout the study area (see area delimited by black dashed lines in Fig. 10). It should be noted that the highest-susceptibility areas are not isolated but rather these are always flanked by high-susceptibility (0.025–0.04 SI units) blocks (Fig. 7, supplementary Figs. S1, S2, S3). Within the basement, the increase of magnetic susceptibility is modelled also by including slight increases of the density of the modelled blocks. The density of the basement ranges between 2700 and 2750 kg m^{-3} corresponding to minimum (0.001 SI units in the upper basement) and maximum (0.05 SI units) magnetic susceptibilities respectively. Such a wide distribution of high-susceptibility volumes suggests a regional-scale phenomenon and excludes that high-magnetic anomalies are associated with scattered sources such, for example, as local intrusions within the crust. A similar configuration is also evident in the northern sector of NNS (East Shetland Basin area), located at ~60 km NNE of our study area. In this zone, Fichler et al. (2011) located high-susceptibility bodies within the crust (red dashed line in Fig. 10) by combining forward modelling of gravity and magnetic anomalies. These authors interpret such bodies as a combination of intermediate intrusives and mantle serpentinization in an island-arc system pertaining to the Iapetus Ocean whose offshore continuation is still debated. Such interpretation is also in agreement with previous studies investigating the Viking Graben and the NNS (Hollinger and Klemperert, 1989; Fichler and Hospers, 1990) where magnitudes and wavelengths of the magnetic anomalies are very similar to those in our study area. Considering their densities and magnetic susceptibilities, the serpentinized blocks we model should range between 40% and 80% of serpentinized fraction (e.g. Fig. 8 in Fichler et al., 2011), similarly to what proposed for the East Shetland Basin area in the NNS (Fichler et al., 2011).

A similar interpretation for the GESP has been proposed by Patruno et al. (2017) and Scisciani et al. (2019). These authors note that the crystalline basement in the study area can be divided into a shallower, acoustically opaque part, largely composed by granitoid and alkaline rocks, as suggested by several partial well penetrations (Kombrink and Patruno, 2020), and by a deeper, reflective layer showing high amplitude and low frequency content. This intra-basement reflective layer (‘*high-reflective deep-seated package*’ in Patruno et al., 2017) has been fortuitously penetrated by at least one well (9/04a-1 – Fig. 10), which reported ‘hornblend-biotite gneiss or shists’ with a metamorphic cooling age of 393 Ma (Early Devonian – Bassett, 2003; Patruno et al., 2017; Scisciani et al., 2019). This deep reflector was therefore interpreted by Patruno et al. (2017) as a regional-wide transition between major crystalline units characterized by substantially different composition and acoustic impedance values (e.g., granites over gneiss, or acidic crystalline rocks over Iapetus-domain meta-basalts, as suggested by the hornblend-biotite mineralogy – Patruno et al., 2017).

Interestingly, the blocks we modelled with the maximum magnetic susceptibility, often correspond to areas of anomalous crustal reflectivity in the analyzed seismic profiles (examples are given in Fig. 11) at TWT depth $\geq$ 5 s. Analogous, intra-basement areas of anomalously-high crustal reflectivity were described by Patruno et al. (2017) and Scisciani et al. (2019) in a shallower sector beneath the Crawford-skipper Basin, Beryl Basin and Fladen Gound Spur, but it seems that similar basement seismic facies can be observed throughout the NNS (Fazlikhani et al., 2017). These strong reflections were variously interpreted by previous authors as: i) crustal blocks and terranes inherited from the Caledonian orogeny (Freeman et al., 1988); ii) crustal-scale fault zones developed

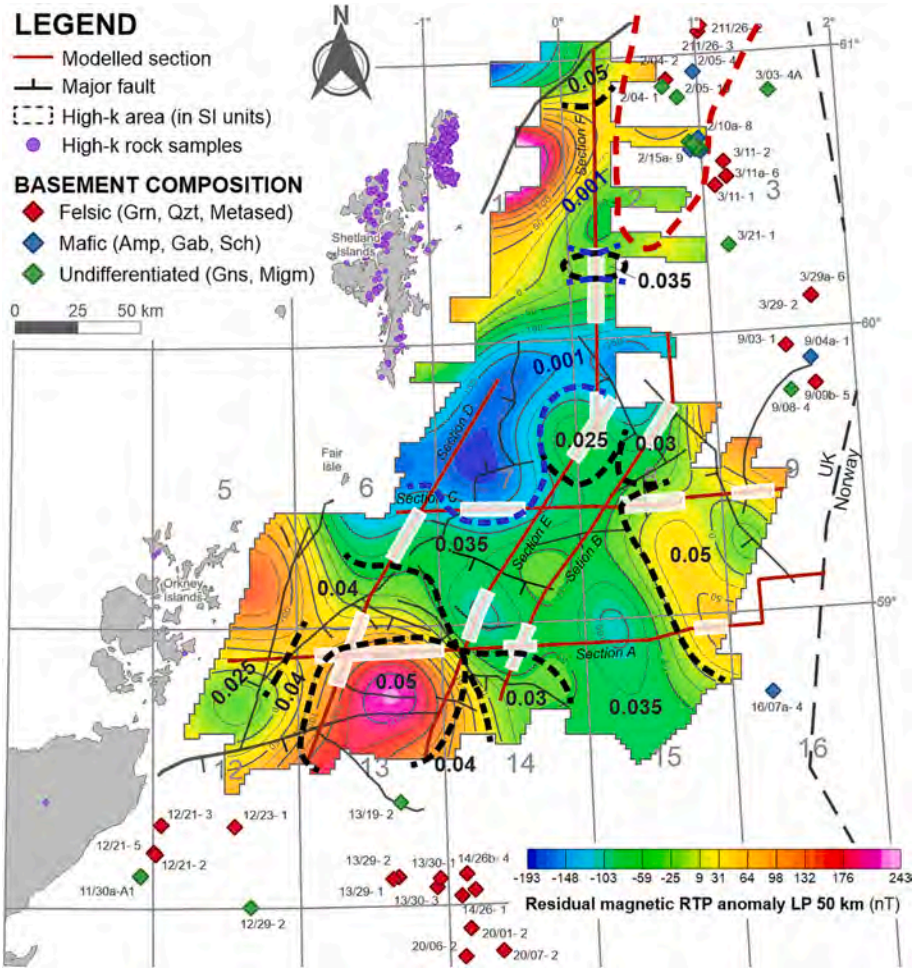

Fig. 10. Filtered magnetic dataset (50 km LP filtering of the RTP magnetic anomaly). The thick dashed lines provide a 15 km-depth slice of the distribution of the magnetic susceptibilities of the basement. Black dashed lines enclose volumes with high susceptibility basement (0.025–0.05 SI units), while the thick blue dashed line encloses the area with low-susceptibility basement (0.001 SI units). The thick dashed red line encompasses the area proposed as serpentinized crust by Fichler et al. (2011). White transparent polygons along the modelled profiles (red lines) enclose areas of high reflectivity matching with high-susceptibility volumes. High-k rock samples refer to onshore gabbroid or serpentinized rocks (BGS, 2022). Diamonds locate well cores that sampled the basement, classified according to Bassett (2003). Contour spacing of the basemap is 25 nT. Structural elements are modified from Scisciani et al. (2021). See Fig. 1b for seismic lines labels. Abbreviations: Grn, granite; Qzt, quartzite; Metased, meta sediment; Amp, amphibolite; Gab, gabbro; Sch, schist; Gns, gneiss; Migm, migmatite. (For interpretation of the references to colour in this figure legend, the reader is referred to the web version of this article.)

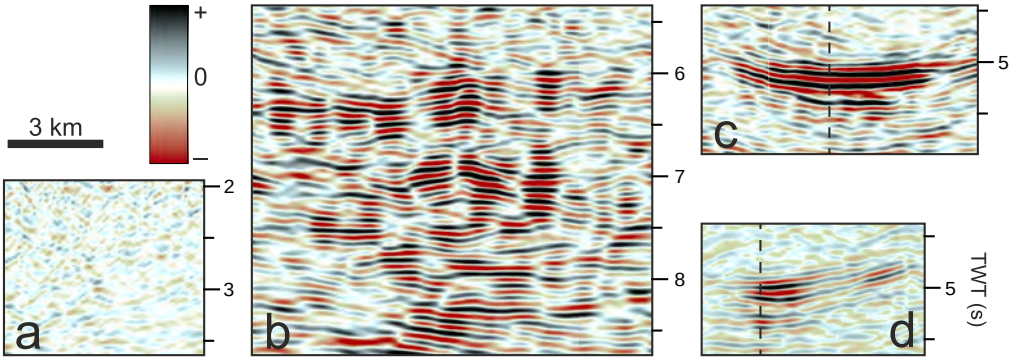

Fig. 11. Portions of seismic reflection profiles showing the different reflectivity of basement and crust in the study area. (a) Low-reflectivity zones (i.e. areas with low-amplitude and discontinuous reflections) match with zones of low magnetic anomaly. Conversely, low-frequency high-reflectivity intervals (b, c and d) generally correspond to high-susceptibility bodies modelled in this work. Dashed lines indicate profile intersection. See Figs. 7 and 8 for location in sections A and B.

during the Mesozoic rifting (e.g., Bell et al., 2014; Phillips et al., 2019); or iii) Mesozoic or Tertiary magmatic intrusions related to the North Sea rift and North-Atlantic opening (Tankard and Balkwill, 1989). Since there is no evidence throughout the GESP or the East Shetland Basin (Fichler et al., 2011) of recent volcanic activity and considering the significant distance of the GESP from the Jurassic-Lower Cretaceous rifting zones to the east, the latter hypothesis can be ruled out. The observed crustal reflectivity is not limited to few kilometers, as typically imaged in fault-related shear zones (Phillips et al., 2019), but it commonly forms huge crustal volumes adjacent to others with similar size and characterized by low-amplitude and discontinuous-to-reflection-free seismic facies (e.g., Fig. 11a). Given the lack of evidence supporting significant crustal-scale fault zones and the relatively low crustal stretching factors estimated in this area (e.g., Christiansson et al., 2000), also the second hypothesis can be ruled out.

Considering all the above, these strongly-reflective and high-susceptibility volumes ($k \geq 0.04$ SI units) are here interpreted as inherited serpentinized crustal domains that formed in island-arc systems of the Iapetus ocean and, following its closure, were stacked during the Caledonian orogeny. If this interpretation is correct, the areas

depicted by magnetic susceptibility higher than 0.04 SI units, would represent the southwards continuation of the island-arc chain proposed for the East Shetland Basin by Fichler et al. (2011), while the surrounding volumes with magnetic susceptibility of 0.025–0.04 SI units may allocate intermediate intrusives whose emplacement was lateral to the island-arc system pertaining to the Iapetus Ocean (Fichler et al., 2011). Considering that the top of the high-susceptibility volumes within the middle crust ranges between 9 and 20 km depth across all the modelled profiles, a more detailed classification of these volumes in the GESP, perhaps attempting to pin point the buried part of the Iapetus ophiolitic suture, is challenging at the very least since it would require strong independent constraints currently not available. The interpretation we propose, relating high-susceptibility bodies with island-arc systems, would be similar to the one proposed for other crustal frameworks (Mancinelli et al., 2022, and references therein).

An alternative interpretation of such regional-scale high-susceptibility volumes would involve volcanic episodes affecting the entire southern East Shetland Platform between Permian and Cretaceous times. When compared with the model proposed in this work, such volcanic-source scenario would allocate shallower magnetic sources in an alternative but still plausible interpretation. Such wide event(s) would result in widespread and thick deposits leading to a crustal setup similar to the one proposed for the Rattray Volcanic Province (Quirie et al., 2018). However, all the available boreholes within and surrounding the study area never reported of volcanic deposits throughout the drilled Permian-Cretaceous sequences (Figs. 2, 3), an evidence that drove our modelling by avoiding the unsupported volcanic-source model setup.

6. Conclusions

In this work, the first integrated forward modelling of gravity and magnetic anomalies across the Greater East Shetland Platform (GESP) was carried out. In order to investigate this under-explored region of the Northern North Sea, six newly processed seismic reflection profiles were interpreted and depth-converted after well-to-seismic tie; the resulting geological cross sections were compared with the observed Bouguer gravity and magnetic anomalies. The time-to-depth conversion of these seismic profiles, combined with stratigraphy, seismic velocity and bulk density data retrieved from well log analysis, allowed to highlight the spatial and temporal evolution of the major basins (i.e. the East Orkney Basin and the Dutch Bank Basin) and the age/thickness of basin infill.

This first order characterization allowed us to find a spatial relation between the observed gravity anomalies and the Mesozoic sedimentary sequences (Fig. 9). The two prominent gravity lows match with the location of the depocenters of two main extensional intra-platform basins in the area (i.e. the Dutch Bank Basin and East Orkney Basin). In particular, the Dutch Bank Basin undergone a prominent Triassic infilling (Fig. 9c) that, in addition to thinner Jurassic units, contributed to the main gravity low observed on the GESP region. On the contrary, the smaller East Orkney Basin underwent a significant tectonic subsidence in the Lower Cretaceous (Fig. 9b). Similar sedimentary contributions can be envisaged for other smaller basins close to the Shetland Island (e.g., north-east of the East Fair Isle Basin). Bouguer gravity anomaly highs are mostly found in areas where the sedimentary cover is reduced in thickness and mainly consists of Devonian sediments in the south-western part of the study area (e.g., the Caithness Ridge and Fair Isle Platform).

The modelling of the magnetic anomaly revealed two contributors. The upper basement is characterized by low-susceptibility values which are compatible with acoustically-opaque metamorphosed sediments and granitoid/alkaline igneous rocks. High-susceptibility volumes in the basement and lower crust are compatible with mafic bodies and serpentinized crust, that shows in reflection seismic as a widespread high-amplitude and low-frequency layer. These high-susceptibility volumes are the main contributors to the observed magnetic anomaly (Figs. 7, 8, 10, Supplementary Figs. S1-S4) and can be related to structural paleodomains connected to the Caledonian orogeny and the pre-Caledonian Iapetus Ocean. If correct, this interpretation will provide important constraints to the understanding of the geodynamic evolution of the area by locating island-arc crustal remnants that pertained to the Iapetus Ocean.

CRediT authorship contribution statement

Mattia De Luca: Conceptualization, Data curation, Visualization, Writing – original draft, Writing – review & editing. **Paolo Mancinelli:** Data curation, Writing – original draft, Writing – review & editing. **Stefano Patruno:** Data curation, Writing – original draft. **Vittorio Scisciani:** Data curation, Writing – original draft, Writing – review & editing.

Declaration of Competing Interest

The authors declare that they have no known competing financial interests or personal relationships that could have appeared to influence the work reported in this paper.

Data availability

Publicly available datasets were analyzed in this study. All data are available from the UK National Data Repository, North Sea Transition Authority's Open Data and British Geological Survey (BGS) websites. Requests to access the datasets should be directed to https://ndr.nstauthority.co.uk/, https://www.nstauthority.co.uk/data-centre/nsta-open-data/ and https://www.bgs.ac.uk/.

Acknowledgements

The authors would like to express their gratitude to Christine Fichler and an anonymous reviewer for their constructive comments that improved the manuscript. This work was funded by FSE REACT-EU Axis IV.5 PON research and innovation 2014-2020 fund (grant number: DOT1353941-3 - M. De Luca PhD research project) and G. d'Annunzio grants to V. Scisciani and P. Mancinelli. Subsurface data are available to the public through the NSTA's National Data Repository (NDR). We are grateful to S&P Global (The Kingdom Software), Schlumberger (Petrel) and Petroleum Experts (Move) for the software academic licenses provided to the G. d'Annunzio University of Chieti-Pescara, all of which have permitted the interpretation, analysis, and presentation of data.

Appendix A. Supplementary data

Supplementary data to this article can be found online at https://doi.org/10.1016/j.tecto.2023.229980.

References

Abramovitz, T., Thybo, H., 2000. Seismic images of Caledonian, lithosphere-scale collision structures in the southeastern North Sea along Mona Lisa Profile 2. Tectonophysics 317 (1), 27–54. https://doi.org/10.1016/S0040-1951(99)00266-8.

Andrews, I.J., Long, D., Richards, P.C., Thomson, A.R., Brown, S., Chesher, J.A., McCormac, M., 1990. The Geology of the Moray Firth. HMSO, London, UK, p. 96 (United Kingdom Offshore Regional Report, 3).

Armitage, T.B., Watts, L.M., Holdsworth, R.E., Strachan, R.A., 2021. Late Carboniferous dextral transpressional reactivation of the crustal-scale Walls Boundary Fault, Shetland: the role of pre-existing structures and lithological heterogeneities. J. Geol. Soc. Lond. 178 https://doi.org/10.1144/jgs2020-078.

Arsenikos, S., Quinn, M.F., Johnson, K., Sankey, M., Monaghan, A.A., 2016. Seismic interpretation and generation of key depth structure surfaces within the Carboniferous and Devonian of the Orcadian Study Area, Quadrants 7-9, 11-15 and 19-21. In: British Geological Survey Commissioned Report, 59pp., CR/16/033. http://nora.nerc.ac.uk/id/eprint/516771.

Arsenikos, S., Quinn, M., Kimbell, G., Williamson, P., Pharaoh, T., Leslie, G., Monaghan, A., 2018. Structural development of the Devono-Carboniferous plays of the UK North Sea. In: Monaghan, A.A., Underhill, J.R., Hewett, A.J., Marshall, J.E.A.

(Eds.), Paleozoic Plays of NW Europe. Geological Society, London, Special Publications, 471, p. 65. https://doi.org/10.1144/SP471.3 (1).
Atherton, M.P., Ghani, A.A., 2002. Slab breakoff: a model for Caledonian, late Granite syn-collisional magmatism in the orthotectonic (metamorphic) zone of Scotland and Donegal, Ireland. Lithos 62, 65–85. https://doi.org/10.1016/S0024-4937(02)00111-1.
Bassett, M.G., 2003. Sub-Devonian geology. In: Evans, D., Graham, C., Armour, A., Bathurst, P. (Eds.), The Millennium Atlas: Petroleum Geology of the Central and Northern North Sea. Geological Society, London, pp. 61–63.
Baykiev, E., Guerri, M., Fullea, J., 2018. Integrating gravity and surface elevation with magnetic data: mapping the curie temperature beneath the British Isles and surrounding areas. Front. Earth Sci. 6 https://doi.org/10.3389/feart.2018.00165.
Beamish, D., Smythe, D.K., 1986. Geophysical images of the deep crust: the Iapetus suture. J. Geol. Soc. 143 (3), 489–497. https://doi.org/10.1144/gsjgs.143.3.0489.
Beamish, D., Kimbell, G., Pharoah, T.C., 2016. The deep crustal magnetic structure of Britain. Proc. Geol. Assoc. 127 (3–4), 647–663. https://doi.org/10.1016/j.pgeola.2016.10.007.
Bell, R.E., Jackson, C.A.L., Whipp, P.S., Clements, B., 2014. Strain migration during multiphase extension: observations from the northern North Sea. Tectonics 33 (10), 1936–1963. https://doi.org/10.1002/2014TC003551.
BGS, 2022. https://mapapps2.bgs.ac.uk/geoindex/home.html (Last visited on October 19, 2022).
Bird, P.C., Cartwright, J.A., Davies, T.L., 2015. Basement reactivation in the development of rift basins: an example of reactivated Caledonide structures in the West Orkney Basin. J. Geol. Soc. Lond. 172 (1), 77–85. https://doi.org/10.1144/jgs2013-098.
Bliss, K., Weston, J., Croft, M., 2016. Processing Report 2d Marine Gravity and magnetic Data OA16ESP, East Shetland Platform Offshore, UK. In: Bridgeporth Prj n16_030, Bridgeporth Ltd.
Chew, D.M., Daly, J.S., Magna, T., Page, L.M., Kirkland, C.L., Whitehouse, M.J., Lam, R., 2010. Timing of ophiolite obduction in the Grampian orogen. Geol. Soc. Am. Bull. 122, 1787–1799. https://doi.org/10.1130/B30139.1.
Christiansson, P., Faleide, J.I., Berge, A.M., 2000. Crustal structure in the northern North Sea: an integrated geophysical study. In: Nottvedt, A., et al. (Eds.), Dynamics of the Norwegian Margin. Geological Society, London, Special Publications, 167, pp. 15–40. https://doi.org/10.1144/GSL.SP.2000.167.01.02.
Claringbould, J.S., Bell, R.E., Jackson, C.A.L., Gawthorpe, R.L., Odinsen, T., 2017. Pre-existing normal faults have limited control on the rift geometry of the northern North Sea. Earth Planet. Sci. Lett. 475, 190–206. https://doi.org/10.1016/j.epsl.2017.07.014.
Coward, M.P., Enfield, M.A., Fischer, M.W., 1989. Devonian basins of Northern Scotland: extension and inversion related to late Caledonian-Variscan tectonics. In: Cooper, M. A., Williams, G.D. (Eds.), Inversion Tectonics. Geological Society, London, Special Publications, 44, pp. 275–308. https://doi.org/10.1144/GSL.SP.1989.044.01.16.
Coward, M.P., Dewey, J.F., Hempton, M., Holroyd, J., 2003. Tectonic evolution. In: Evans, D., et al. (Eds.), The Millennium Atlas: Petroleum Geology of the Central and Northern North Sea. The Geological Society, London, vol. 17, p. 33.
Crowley, Q.G., Strachan, R.A., 2015. U–Pb zircon constraints on obduction initiation of the Unst Ophiolite: an oceanic core complex in the Scottish Caledonides? J. Geol. Soc. 172, 279–282. https://doi.org/10.1144/jgs2014-125.
Davies, R.J., O'Donnell, D., Bentham, P., Gibson, J.P.C., Curry, M.R., Dunay, R.E., Maynard, J.R., 1999. The origin and genesis of major Jurassic unconformities within the triple junction area of the North Sea, UK. In: Fleet, A.J., Boldy, S.A.R. (Eds.), Petroleum Geology Conference Series, the Geological Society, London, vol. 5, pp. 117–131. https://doi.org/10.1144/0050117.
Dewey, J.F., Shackleton, R.J., 1984. A model for the evolution of the Grampian tract in the early Caledonides and Appalachians. Nature 312, 115–120. https://doi.org/10.1038/312115a0.
Dewey, J.F., Strachan, R.A., 2003. Changing Silurian–Devonian relative plate motion in the Caledonides: sinistral transpression to sinistral transtension. J. Geol. Soc. Lond. 160, 219–229. https://doi.org/10.1144/0016-764902-085.
Dewey, J.F., Dalziel, I.W., Reavy, R.J., Strachan, R.A., 2015. The Neoproterozoic to Mid-Devonian evolution of Scotland: a review and unresolved issues. Scott. J. Geol. 51, 5–30. https://doi.org/10.1144/sjg2014-007.
Donato, J.A., Tully, M.C., 1982. A proposed granite batholith along the western flank of the North Sea Viking Graben. Geophys. J. R. Astron. Soc. 69, 187–195. https://doi.org/10.1111/j.1365-246X.1982.tb04943.x.
Düzgit, Z., Hisarli, M., Sayin, N., Orbay, N., 2006. Correlation between gravity and magnetic anomalies of Western Anatolia and its relation to tectonic structures. Earth Planets Space 58, 943–949. https://doi.org/10.1186/BF03352599.
Etris, E.L., Crabtree, N.J., Dewar, J., 2002. True Depth-conversion: more than a Pretty Picture. Scott Pickford, A Core Laboratories Company 26 (9).
Færseth, R.B., 1996. Interaction of Permo-Triassic and Jurassic extensional fault-blocks during the development of the northern North Sea. J. Geol. Soc. Lond. 153, 931–944. https://doi.org/10.1144/gsjgs.153.6.0931.
Fazlikhani, H., Fossen, H., Gawthorpe, R.L., Faleide, J.I., Bell, R.E., 2017. Basement structure and its influence on the structural configuration of the northern North Sea rift. Tectonics 36, 1151–1177. https://doi.org/10.1002/2017TC004514.
Fichler, C., Hospers, J., 1990. Deep crustal structure of the northern North Sea Viking Graben: results from deep reflection seismic and gravity data. Tectonophysics 178, 241–254. https://doi.org/10.1016/0040-1951(90)90150-7.
Fichler, C., Pastore, Z., 2022. Petrology of the crystalline crust in the southwestern Barents Sea inferred from geophysical data. Nor. J. Geol. 102, 43. https://doi.org/10.17850/njg102-2-2.
Fichler, C., Odinsen, T., Rueslåtten, H., Olesen, O., Vindstad, J.E., Wienecke, S., 2011. Crustal inhomogeneities in the Northern North Sea from potential field modelling: inherited structure and serpentinites? Tectonophysics 510, 172–185. https://doi.org/10.1016/j.tecto.2011.06.026.
Flinn, D., 1961. Continuation of the Great Glen Fault beyond the Moray Firth. Nature 191, 589–591. https://doi.org/10.1038/191589b0.
Flinn, D., 1992. The history of the Walls Boundary fault, Shetland: the northward continuation of the Great Glen fault from Scotland. J. Geol. Soc. Lond. 149, 721–726. https://doi.org/10.1144/gsjgs.149.5.0721.
Flinn, D., 1996. The Shetland Ophiolite complex: field evidence for the intrusive emplacement of the 'cumulate' layers. Scott. J. Geol. 32, 151–158. https://doi.org/10.1144/sjg32020151.
Flinn, D., 1999. The Shetland Ophiolite. In: Stephenson, D., Bevins, R.E., Millward, D., Highton, A.J., Parsons, I., Stone, P., Wadsworth, W.J. (Eds.), Caledonian Igneous Rocks of Great Britain. Joint Nature Conservation Committee. Geological Conservation Review Series, vol. 17, pp. 31–58.
Flinn, D., 2001. The basic rocks of the Shetland Ophiolite complex and their bearing on its genesis. Scott. J. Geol. 37, 79–96. https://doi.org/10.1144/sjg37020079.
Flinn, D., Oglethorpe, R.J.D., 2005. A history of the Shetland Ophiolite complex. Scott. J. Geol. 41, 141–148. https://doi.org/10.1144/sjg41020141.
Flinn, D., Stone, P., Stephenson, D., 2013. The Dalradian rocks of the Shetland Islands, Scotland. Proc. Geol. Assoc. 124 (1–2), 393–409. https://doi.org/10.1016/j.pgeola.2012.07.007.
Fossen, H., 1992. The role of extensional tectonics in the Caledonides of South Norway. J. Struct. Geol. 14, 1033–1046. https://doi.org/10.1016/0191-8141(92)90034-T.
Fossen, H., 2010. Extensional tectonics in the North Atlantic Caledonides: a regional view. In: Law, R.D., Butler, R.W.H., Holdsworth, R.E., Krabbendam, M., Strachan, R. A. (Eds.), Continental Tectonics and Mountain Building: the Legacy of Peach and Horne. Geological Society, London, Special Publications, 335, pp. 767–793. https://doi.org/10.1144/sp335.31.
Fossen, H., Hurich, C.A., 2005. The Hardangerfjord Shear Zone in SW Norway and the North Sea: a large- scale low-angle shear zone in the Caledonian crust. J. Geol. Soc. Lond. 162, 675–687. https://doi.org/10.1144/0016-764904-136.
Fossen, H., Fazlikhani, H., Faleide, J.I., Ksienzyk, A.K., Dunlap, W.J., 2016. Post-Caledonian extension in the West Norway–northern North Sea region: the role of structural inheritance. Geol. Soc. Lond., Spec. Publ. 439, 465–486. https://doi.org/10.1144/SP439.6.
Fraser, S., Robinson, A., Johnson, H., Underhill, A., Kadolsky, D., 2003. Upper Jurassic. In: Evans, D., Graham, C., Armour, A., Bathurst, P. (Eds.), The Millennium Atlas: Petroleum Geology of the Central and Northern North Sea. Geological Society, London, pp. 157–189.
Freeman, B., Klemperer, S.L., Hobbs, R.W., 1988. The deep structure of northern England and the Iapetus Suture zone from BIRPS deep seismic reflection profiles. J. Geol. Soc. Lond. 145 (5), 727–740. https://doi.org/10.1144/gsjgs.145.5.0727.
Frogtech Geoscience, 2017. 21 CXRM East Shetland Platform Project Phase 1 - SEEBASE Study. Frogtech Pty Ltd, Canberra, Australia.
Garland, G.D., 1951. Combined analysis of gravity and magnetic anomalies. Geophysics 16 (1), 51–62. https://doi.org/10.1190/1.1437650.
Glennie, K.W., Underhill, J.R., 1998. Development and evolution of structural styles. In: Glennie, K.W. (Ed.), Petroleum Geology of the North Sea: Basic Concepts and Recent Advances. Blackwell Science, Oxford, UK, pp. 42–84. https://doi.org/10.1002/9781444313413.ch2.
Glennie, K.W., Higham, J., Stemmerik, L., 2003. Permian. In: Evans, D., Graham, C., Armour, A., Bathurst, P. (Eds.), The Millennium Atlas: Petroleum Geology of the Central and Northern North Sea. Geological Society, London, pp. 91–103.
Glover, P.W.J., 2000. Petrophysics – MSc Petroleum Geology. Department of Geology and Petroleum Geology, University of Aberdeen, UK, p. 376.
Goldsmith, P.J., Hudson, G., Van Veen, P., 2003. Triassic. In: Evans, D., Graham, C., Armour, A., Bathurst, P. (Eds.), The Millennium Atlas: Petroleum Geology of the Central and Northern North Sea. Geological Society, London, pp. 105–127.
Gradmann, S., Ebbing, J., Fullea, J., 2013. Integrated geophysical modelling of a lateral transition zone in the lithospheric mantle under Norway and Sweden. Geophys. J. Int. 194 (3), 1358–1373. https://doi.org/10.1093/gji/ggt213.
Harper, M., 1971. Approximate geothermal gradients in the North Sea Basin. Nature 230, 235–236. https://doi.org/10.1038/230235a0.
Holliger, K., Klemperer, S., 1989. A comparison of the Moho interpreted from gravity data and from deep seismic reflection data in the Northern North Sea. Geophys. J. 97, 247–258. https://doi.org/10.1111/j.1365-246X.1989.tb00499.x.
Holliger, K., Klemperer, S., 1990. Gravity and deep seismic reflection profiles across the North Sea rifts. In: Blundell, D.J., Gibbs, A. (Eds.), Tectonic Evolution of the North Sea Rifts. Oxford University Press, Oxford, UK, pp. 82–100.
Holloway, S., Reay, D.M., Donato, J.A., Beddoe-Stephens, B., 1991. Distribution of granite and possible Devonian sediments in part of the East Shetland Platform, North Sea. J. Geol. Soc. 148, 635–638. https://doi.org/10.1144/gsjgs.148.4.0635.
Hutton, D.H.W., McErlean, M., 1991. Silurian and early Devonian sinistral deformation of the Ratagain granite, Scotland: constraints on the age of Caledonian movements on the Great Glen Fault system. J. Geol. Soc. Lond. 148 (1), 1–4. https://doi.org/10.1144/gsjgs.148.1.0001.
Johnson, H., Leslie, A.B., Wilson, C., Andrews, I., Cooper, R.M., 2005. Middle Jurassic, Upper Jurassic and Lower Cretaceous of the UK Central and Northern North Sea. In: BGS Research Report, RR/03/001, Keyworth. https://nora.nerc.ac.uk/id/eprint/3680.
Karstens, J., Müller, P., Berndt, C., Patruno, S., 2022. Deep-seated focused fluid migration as indicator for hydrocarbon leads in the East Shetland Platform, North Sea Province. In: Patruno, S., Archer, S.G., Chiarella, D., Howell, J.A., Jackson, C.A.-L., Kombrink, H. (Eds.), Cross-Border Themes in Petroleum Geology I: The North Sea, vol. 494. Geological Society Special Publications, The Geological Society, London, United Kingdom, pp. 461–480. https://doi.org/10.1144/SP494-2019-26.

Kearey, P., Brooks, M., Hill, I., 2002. An Introduction to Geophysical Exploration, Third edition. Blackwell Science Ltd. ISBN 0–632–04929-4.
Kendall, R.S., 2017. The Old Red Sandstone of Britain and Ireland — a review. Proc. Geol. Assoc. 128 (3), 409–421. https://doi.org/10.1016/j.pgeola.2017.05.002.
Kimbell, G.S., Williamson, J.P., 2016. A gravity interpretation of the Orcadian Basin area. In: British Geological Survey Commissioned Report, CR/16/034, p. 50.
Kombrink, H., Patruno, S., 2020. The integration of public domain lithostratigraphic data into a series of cross-border North Sea well-penetration maps. Geol. Soc. Lond., Spec. Publ. 494 https://doi.org/10.1144/SP494-2020-25.
Lambert, R.J. St, McKerrow, W.S., 1976. The Grampian Orogeny. Scott. J. Geol. 12, 271–292. https://doi.org/10.1144/sjg12040271.
Le Breton, E., Cobbold, P.R., Zanella, A., 2013. Cenozoic reactivation of the Great Glen Fault, Scotland: additional evidence and possible causes. J. Geol. Soc. Lond. 170, 403–415. https://doi.org/10.1144/jgs2012-067.
Lyngsie, S.B., Thybo, H., 2007. A new tectonic model for the Laurentia–Avalonia–Baltica suture in the North Sea: a case study along MONA LISA profile 3. Tectonophysics 429, 201–227. https://doi.org/10.1016/j.tecto.2006.09.017.
Mancinelli, P., Pauselli, C., Fournier, D., Fedi, M., Minelli, G., Barchi, M.R., 2020. Three-dimensional gravity local inversion across the area struck by the 2016-2017 seismic events in Central Italy. Journal of Geophysical Research – Solid. Earth 125 (2). https://doi.org/10.1029/2019JB018853.
Mancinelli, P., Scisciani, V., Pauselli, C., Stampfli, G.M., Speranza, F., Vasiljevic, I., 2022. Back-arc underplating provided crustal accretion affecting topography and sedimentation in the Adria microplate. Mar. Pet. Geol. 136, 105470 https://doi.org/10.1016/j.marpetgeo.2021.105470.
Marshall, J.E.A., Hewett, A.J., 2003. Devonian. In: Evans, D., Graham, C., Armour, A., Bathurst, P. (Eds.), The Millennium Atlas: Petroleum Geology of the Central and Northern North Sea. Geological Society, London, pp. 65–81.
Marshall, J.E.A., Glennie, K.W., Astin, T.R., Hewett, A.J., 2019. The Old Red Group (Devonian) – Rotliegend (Permian) Unconformity in the Inner Moray Firth. Geol. Soc. Lond., Spec. Publ. 471 (1), 237–252. https://doi.org/10.1144/SP471.12.
McBride, J.H., England, R.W., 1999. Window into the Caledonian orogen: Structure of the crust beneath the East Shetland platform, United Kingdom. Geol. Soc. Am. Bull. 111, 1030–1041. https://doi.org/10.1130/0016-7606(1999)111<1030:WITCOS>2.3.CO;2.
McClay, K.R., Norton, M.G., Coney, P., Davis, G.H., 1986. Collapse of the Caledonian orogeny and the old red sandstone. Nature 323, 147–149. https://doi.org/10.1038/323147A0.
Mendum, J.R., Noble, S.R., 2010. Mid-Devonian sinistral transpressional movements on the Great Glen Fault: The rise of the RosemarkieInlier and the Acadian Event in Scotland. In: Continental Tectonics and Mountain Building: The Legacy of Peach and Horne, 335. Geological Society Special Publlication, pp. 161–187. https://doi.org/10.1144/SP335.8.
Norton, M.G., 1987. The Nordfjord-Sogn Detachment, W Norway. Nor. J. Geol. 67, 93–106.
Nøttvedt, A., Gabrielsen, R.H., Steel, R.J., 1995. Tectonostratigraphy and sedimentary architecture of rift basins, with reference to the Northern North Sea. Mar. Pet. Geol. 12, 881–901. https://doi.org/10.1016/0264-8172(95)98853-W.
NSTA, 2017. https://www.nstauthority.co.uk/news-publications/news/2017/gov-funded-seismic-data-launch/ (last visited October 19, 2022).
NSTA, 2022. UK National Data Repository (NDR). Available at. https://ndr.nstauthority.co.uk/ (last visited October 19, 2022).
Osmundsen, P.T., Andersen, T.B., Markussen, S., Svendby, A.K., 1998. Tectonics and sedimentation in the hangingwall of a major extensional detachment: the Devonian Kvamshesten Basin, western Norway. Basin Res. 10, 213–234. https://doi.org/10.1046/j.1365-2117.1998.00064.x.
Patruno, S., Reid, W., 2016. New plays on the Greater ESP (UKCS Quadrants 3, 8-9, 14-16) – Part 1: Regional setting and a working petroleum system. First Break 34, 33–45. https://doi.org/10.3997/1365-2397.2016016.
Patruno, S., Reid, W., 2017. New plays on the Greater ESP (UKCS Quadrants 3, 8–9, 14–16) – Part 2: Newly reported Permo-Triassic intra-platform basins and their influence on the Devonian–Paleogene prospectivity of the area. First Break 35, 59–69. https://doi.org/10.3997/1365-2397.2016017.
Patruno, S., Scisciani, V., 2021. Testing normal fault growth models by seismic stratigraphic architecture: the case of the Pliocene-Quaternary Fucino Basin (Central Apennines, Italy). Basin Res. 33 (3), 2118–2156. Wiley. https://doi.org/10.1111/bre.12551.
Patruno, S., Gall, M., Scisciani, V., 2017. Newly-observed Caledonian and Devonian fold and thrust structures in the UK North Sea, 'Fold and Thrust belts: structural style, evolution and exploration' Conference, Geological Society London, London, United Kingdom, 31 October – 2 November 2017. Abstract and Poster Presentation.
Patruno, S., Reid, W., Berndt, C., Feuilleaubois, L., 2019. Polyphase tectonic inversion and its role in controlling hydrocarbon prospectivity in the Greater ESP and Mid North Sea High, offshore UK. In: Monaghan, A.A., Underhill, J.R., Hewett, A.J., Marshall, J.E.A. (Eds.), Palaeozoic Plays of NW Europe. Geological Society, London, Special Publications, 471, pp. 177–235. https://doi.org/10.1144/SP471.9.
Patruno, S., Kombrink, H., Archer, S.G., 2022. Cross-border megasequence stratigraphy of the Northern, Central and Southern North Sea: A comparative tectono-stratigraphic synthesis. In: Patruno, S., Archer, S.G., Chiarella, D., Howell, J.A., Jackson, C.A.-L., Kombrink, H. (Eds.), Cross-Border Themes in Petroleum Geology I: The North Sea, vol. 494 (1). Geological Society Special Publications, The Geological Society, London, U.K, pp. 13–83. https://doi.org/10.1144/SP494-2020-228.
Pegrum, R.M., Spencer, A.M., 1990. Hydrocarbon plays in the northern North Sea. In: Brooks, J. (Ed.), Classic Petroleum Provinces, 50. Geological Society Special Publication, pp. 441–470. https://doi.org/10.1144/GSL.SP.1990.050.01.27.
PGS, 2017. East Shetland Platform OGA 2D Interpretation Workflow Report. PGS Reservoir (for UK Oil & Gas Authority), March 2017/16.1931. available online at. www.ukoilandgasdata.com/dp/pages/apptab/ITabManager.jsp.
Phillips, T.B., Jackson, C.A.L., Bell, R.E., Duffy, O.B., Fossen, H., 2016. Reactivation of intrabasement structures during rifting: a case study from 1 offshore Norway. J. Struct. Geol. 91, 54–73. https://doi.org/10.1016/j.jsg.2016.08.008.
Phillips, T.B., Fazlikhani, H., Gawthorpe, R.L., Fossen, H., Jackson, C.A.L., Bell, R.E., Faleide, J.I., Rotevatn, A., 2019. The influence of structural inheritance and multiphase extension on rift development, the northern North Sea. Tectonics 38, 4099–4126. https://doi.org/10.1029/2019TC005756.
Platt, N.H., 1995. Structure and tectonics of the northern North Sea: new insights from deep penetration regional seismic data. In: Lambiase, J.J. (ed.), Hydrocarbon Habitat in Rift Basins. J. Geol. Soc. Lond. Spec. Publ. 80 (1), 103–113. https://doi.org/10.1144/GSL.SP.1995.080.01.05.
Platt, N.H., Cartwright, J.A., 1998. Structure of the East Shetland Platform, Northern North Sea. Pet. Geosci. 4 (4), 353–362. https://doi.org/10.1144/petgeo.4.4.353.
Prichard, H.M., Lord, R.A., 1993. An overview of the PGE concentrations in the Shetland ophiolite complex. In: Prichard, H.M., Harris, N.B.W., Neary, C.R. (Eds.), Magmatic Processes and Plate Tectonics, 76. Special Publication of the Geological Society, London, Special Publications, pp. 273–294. https://doi.org/10.1144/GSL.SP.1993.076.01.13 (1).
Quirie, A.K., Schofield, N., Hartley, A., Hole, M.J., Archer, S.G., Underhill, J.R., Watson, D., Holford, S.P., 2018. The Rattray Volcanics: Middle Jurassic fissure volcanism in the UK Central North Sea. J. Geol. Soc. 176 (3), 462. https://doi.org/10.1144/jgs2018-151.
Reynolds, J.M., 2011. An introduction to applied and environmental geophysics. In: John M. Reynolds – 2nd ed. Wiley-Blackwell. ISBN 978-0-471-48535-3.
Richardson, N.J., Alle, M.R., Underhill, J.R., 2005. Role of Cenozoic fault reactivation in controlling pre-rift plays, and the recognition of Zechstein Group evaporite-carbonate lateral facies transitions in the East Orkney and Dutch Bank basins, East Shetland Platform, UK North Sea. In: Geological Society, London, Petroleum Geology Conference Series, 6, pp. 337–348. https://doi.org/10.1144/0060337.
Robert, B., Domeier, M., Jakob, J., 2021. On the origins of the Iapetus Ocean. Earth Sci. Rev. 221, 103791 https://doi.org/10.1016/j.earscirev.2021.103791.
Roberts, A.M., Holdsworth, R.E., 1999. Linking onshore and offshore structures: mesozoic extension in the Scottish Highlands. J. Geol. Soc. Lond. 156, 1061–1064. https://doi.org/10.1144/gsjgs.156.6.1061.
Roberts, A.M., Badley, M.E., Price, J.D., Huck, I.W., 1990. The structural history of a transtensional basin: inner Moray Firth, NE Scotland. J. Geol. Soc. Lond. 147, 87–103. https://doi.org/10.1144/gsjgs.147.1.0087.
Rybakov, M., Goldshmidt, V., Hall, J.K., Ben-Avraham, Z., Lazar, M., 2011. New insights into the sources of magnetic anomalies in the Levant. Russ. Geol. Geophys. 52, 377–397. https://doi.org/10.1016/j.rgg.2011.03.001.
Scisciani, V., Patruno, S., Tavarnelli, E., Calamita, F., Pace, P., Iacopini, D., 2019. Multi-phase reactivations and inversions of Paleozoic–Mesozoic extensional basins during the Wilson cycle: Case studies from the North Sea (UK) and the Northern Apennines (Italy). Geol. Soc. Spec. Publ. 470 (1), 205–243. https://doi.org/10.1144/SP470-2017-232.
Scisciani, V., Patruno, S., D'Intino, N., Esestime, P., 2021. Paleozoic basin reactivation and inversion of the underexplored Northern North Sea platforms: a cross-border approach. Geol. Soc. Lond., Spec. Publ. 494 (1), 301. https://doi.org/10.1144/SP494-2020-252.
Seranne, M., 1992. Devonian extensional tectonics versus Carboniferous inversion in the northern Orcadian basin. J. Geol. Soc. Lond. 149, 27–37. https://doi.org/10.1144/gsjgs.149.1.0027.
Seranne, M., Seguret, M., 1987. The Devonian basins of western Norway: tectonics and kinematics of an extending crust. In: Coward, M.P., Dewey, J.F., Hancock, P.L. (Eds.), Continental Extensional Tectonics. Geological Society, London, Special Publications, 28, pp. 537–548. https://doi.org/10.1144/GSL.SP.1987.028.01.35.
Seranne, M., Chauvet, A., Seguret, M., Brunel, M., 1989. Tectonics of the Devonian collapse basins of western Norway. Bulletin de la Société Géologique de France 5, 489–499. https://doi.org/10.2113/gssgfbull.V.3.489.
Smallwood, J.R., White, R.S., 2002. Ridge-plume interaction in the North Atlantic and its influence on continental breakup and seafloor spreading. In: Jolley, D.W., Bell, B.R. (Eds.), The North Atlantic Igneous Province: Stratigraphy, Tectonic, Volcanic and Magmatic Processes, Geological Society, vol. 197. Special Publications, London, pp. 15–37. https://doi.org/10.1144/GSL.SP.2002.197.01.02.
Smallwood, J.R., Staples, R.K., Richardson, K.R., White, R.S., 1999. Crust generated above the Iceland mantle plume: from continental rift to oceanic spreading center. J. Geophys. Res. 104 (B10), 22885–22902. https://doi.org/10.1029/1999JB900176.
Soper, N.J., England, R.W., 1995. Vendian and Riphean rifting in NW Scotland. J. Geol. Soc. 152 (1), 11–14. https://doi.org/10.1144/gsjgs.152.1.0011.
Soper, N.J., England, R.W., Snyder, D.B., Ryan, P.D., 1992. The lapetus suture zone in England, Scotland and eastern Ireland: a reconciliation of geological and deep seismic data. J. Geol. Soc. Lond. 149 (5), 697–700. https://doi.org/10.1144/gsjgs.149.5.0697.
Steel, R.J., 1993. Triassic-Jurassic megasequence stratigraphy in the Northern North Sea: rift to post-rift evolution. Geol. Soc. Lond. Petrol. Geol. Conf. Ser. 4, 299–315. https://doi.org/10.1144/0040299.
Steel, R.J., Ryseth, A., 1990. The Triasssic–early Jurassic succession in the northern North Sea: megasequence stratigraphy and intra-Triassic tectonics. In: Hardmanr, P. F., Brooks, J. (Eds.), Tectonic Events Responsible for Britain's Oil and Gas Reserves. Geological Society, London, Special Publications, 55, pp. 139–168. https://doi.org/10.1144/GSL.SP.1990.055.01.07.

Steel, R., Siedlecka, A., Roberts, D., 1985. The Old Red Sandstone basins of Norway and their deformation: A review. In: Gee, D., Sturt, B.A. (Eds.), The Caledonian Orogen: Scandinavia and Related Areas. John Wiley, Chichester, UK, pp. 293–315.

Stewart, M.A., Strachan, R.A., Holdsworth, R.E., 1997. Direct field evidence for sinistral displacements along the Great Glen Fault Zone: late Caledonian reactivation of a regional basement structure? J. Geol. Soc. Lond. 154, 135–139. https://doi.org/10.1144/gsjgs.154.1.0135.

Stewart, M.A., Strachan, R.A., Holdsworth, R.E., 1999. Structure and early kinematic history of the Great Glen Fault Zone, Scotland. Tectonics 18 (2), 326–342. https://doi.org/10.1029/1998TC900033.

Strachan, R.A., Woodcock, N.H., 2021. The Tectonic Pattern of Britain and Ireland. Encyclopedia of Geology (Second Edition), pp. 328–337. https://doi.org/10.1016/B978-0-12-409548-9.12412-1.

Strachan, R.A., Smith, M., Harris, A.L., Fettes, D.J., 2002. The Northern Highland and Grampian terranes. In: Trewin, N.H. (Ed.), The Geology of Scotland, 4th edition. The Geological Society, London, pp. 81–148. https://doi.org/10.1144/GOS4P.4.

Tankard, A.J., Balkwill, H.R., 1989. Extensional tectonics and stratigraphy of the North Atlantic margins. AAPG Mem. 46 https://doi.org/10.1306/M46497.

Telford, W.M., Geldart, L.P., Sheriff, R.E., 1990. Applied Geophysics, 2nd ed. Press Syndicate of the University of Cambridge. ISBN 0–521–32693-1.

Turner, C.C., Cronin, B.T., Riley, L.A., Patruno, S., Reid, W.T.L.R., Hoth, S., Knaust, D., Allerton, S., Jones, M.A., Jackson, C.A.-L., 2018. The South Viking Graben: Overview of Upper Jurassic rift geometry, biostratigraphy and extent of Brae Play submarine fan systems. In: Turner, Colin C., Cronin, Bryan T. (Eds.), Rift-related coarse-grained submarine fan reservoirs; the Brae Play, South Viking Graben, North Sea: American Association of Petroleum Geologists (AAPG) Memoir, 115, pp. 9–38. http://archives.datapages.com/data/aapg-books-aop/rift-related-coarse-grained-submarine-fan-reservoirs-the-brae-play-south-viking-graben-north-sea-memoir-115/13652177m1153807.html.

Underhill, J.R., Brodie, J.A., 1993. Structural geology of Easter Ross, Scotland: implications for movement on the Great Glen fault zone. J. Geol. Soc. Lond. 150, 515–527. https://doi.org/10.1144/gsjgs.150.3.0515.

Underhill, J.R., Partington, M.A., 1993. Jurassic thermal doming and deflation in the North Sea: implication of the sequence stratigraphic evidence. In: Parker, J.R. (Ed.), Petroleum Geology of Northwest Europe: Proceedings of the 4th Conference, The Geological Society, London, United Kingdom, 4, pp. 337–345. https://doi.org/10.1144/0040337.

Vetti, V.V., Fossen, H., 2012. Origin of contrasting Devonian supradetachment basin types in the Scandinavian Caledonides. Geology 40, 571–574. https://doi.org/10.1130/G32512.1.

Wasilewski, P.J., Mayhew, M.A., 1992. The Moho as a magnetic boundary revisited. Geophys. Res. Lett. 19 (22), 2259–2262. https://doi.org/10.1029/92GL01997.

Wasilewski, P.J., Thomas, H.H., Mayhew, M.A., 1979. The Moho as a magnetic boundary. Geophys. Res. Lett. 6 (7), 541–544. https://doi.org/10.1029/GL006i007p00541.

Whitbread, K., Kearsey, T., 2016. Devonian and Carboniferous stratigraphical correlation and interpretation in the Orcadian area, Central North Sea, Quadrants 7–22. In: British Geological Survey Commissioned Report, CR/16/032, p. 74. http://nora.nerC.aC.uk/516770/.

White, N., 1989. Nature of lithospheric extension in the North Sea. Geol. Geolog. Soc. Am. 17 (2), 111–114. https://doi.org/10.1130/0091-7613(1989)017<0111:NOLEIT>2.3.CO;2.

Williams, H., Smyth, W.R., 1973. Metamorphic aureoles beneath ophiolite suites and alpine peridotites; tectonic implications with West Newfoundland examples. Am. J. Sci. 273 (7), 594–621. https://doi.org/10.2475/ajs.273.7.594.

Basement-influenced rifting and basin development: a reappraisal of post-Caledonian faulting patterns from the North Coast Transfer Zone, Scotland. In: Wilson, R.W., Holdsworth, R.E., Wild, L.E., McCaffrey, K.J.W., England, R.W., Imber, J., Strachan, R.A., Law, R.D., Butler, R.W.H., Holdsworth, R.E., Krabbendam, M., Strachan, R.A. (Eds.), 2010. Continental Tectonics and Mountain Building: The Legacy of Peach and Horne. Geological Society, London, 335. Special Publications, pp. 795–826. https://doi.org/10.1144/SP335.32.

Zanella, E., Coward, M.P., 2003. Structural framework. In: Evans, D., Graham, D., Armour, A., Bathurst, P. (Eds.), The Millennium Atlas: Petroleum Geology of the Central and Northern North Sea. The Geological Society of London, London, pp. 45–59.

Ziegler, P.A., 1975. Geologic evolution of the North Sea and its tectonic framework Am. Assoc. Petrol. Geol. Bulletin 59, 1073–1097.

Ziegler, P.A., 1992. North Sea rift system. Tectonophysics 208, 55–75. https://doi.org/10.1016/0040-1951(92)90336-5.